European Journal of Pharmaceutical Sciences 212 (2025) 107187

Contents lists available at ScienceDirect

European Journal of Pharmaceutical Sciences

journal homepage: www.elsevier.com/locate/ejps

Comparative study of multidrug resistance-targeting 8-hydroxyquinoline-amino acid conjugates: anticancer effect, interaction with human serum albumin and organic anion transporting polypeptides

Orsolya Dömötör [a,*], Tamás Pivarcsik [a], Zeinab Nezafat Yazdi [b], Éva Bakos [b], Csilla Özvegy-Laczka [b], Anasztázia Hetényi [c], Tamás Martinek [c,d], István Szatmári [e,f], Szilárd Tóth [g,h], Gergely Szakács [g,i], Attila Borics [j,*], Éva A. Enyedy [a]

[a] Department of Molecular and Analytical Chemistry, Interdisciplinary Excellence Centre, University of Szeged, Dóm tér 7-8, H-6720 Szeged, Hungary
[b] Institute of Molecular Life Sciences, RCNS, Eötvös Loránd Research Network, Magyar tudósok krt. 2, H-1117 Budapest, Hungary
[c] Department of Medical Chemistry, University of Szeged, Dóm tér 8, Szeged, Hungary
[d] HUN-REN-SZTE Biomimetic Systems Research Group, Dóm tér 8, Szeged, Hungary
[e] Institute of Pharmaceutical Chemistry, University of Szeged, Eötvös u. 6, H-6720 Szeged, Hungary
[f] HUN REN-SZTE Stereochemistry Research Group, University of Szeged, Eötvös u. 6, H-6720 Szeged, Hungary
[g] Drug Resistance Research Group, Institute of Molecular Life Sciences, HUN-REN Research Centre for Natural Sciences, Magyar tudósok krt. 2, H-1117 Budapest, Hungary
[h] National Laboratory for Drug Research and Development, Magyar tudósok krt. 2, H-1117 Budapest, Hungary
[i] Center for Cancer Research, Medical University of Vienna, Borschkegasse 8a, A-1090 Vienna, Austria
[j] Laboratory of Chemical Biology, Institute of Biochemistry, HUN-REN Biological Research Centre, Szeged, Hungary

ARTICLE INFO

Keywords:
8-hydroxyquinoline
Cytotoxicity
Multidrug resistance
Albumin binding
Proton dissociation
Lipophilicity

ABSTRACT

There is a significant demand for the development of targeted and effective treatments for drug-resistant cancer. We have formerly developed several 8-hydroxyquinoline Mannich base compounds whose toxicity is actually enhanced, rather than diminished on multidrug resistant cancer cells. The scope of our work is to provide comprehensive data on the cytotoxicity of *D/L*-5-chloro- or 5-nitro substituted 7-((homo)proline-1-ylmethyl) quinolin-8-ol compounds on cocultured parental (MES-SA) and ABCB1-expressing MDR (MES-SA/Dx5 and MES-SA/B1) uterine sarcoma cancer cells, to determine the inhibitory effect on organic anion transporting polypeptides (OATPs) OATP1B1 and OATP2B1, and to characterize the solution chemical and human serum albumin (HSA) binding properties of these molecules, thus assessing certain main pharmacokinetic descriptors in absorption and distribution. Although, 5-chloro substituted amino acid conjugates of the Mannich base 8-hydroxyquinoline (HQ) derivatives showed moderate cytotoxicity against the parental cells, their anticancer activity was increased on the MDR cell lines. Proton dissociation constants and distribution coefficients were determined and compared; and HSA binding of these molecules was followed by the combination of UV–vis spectrophotometry, time-resolved and steady state fluorometry, circular dichroism spectroscopy, saturation transfer difference NMR and ultrafiltration. HSA serves as a potential carrier for these amino acid conjugates, with at least two binding sites. The inhibition of OATP1B1 and OATP2B1 was studied *in vitro* and by molecular docking to get an insight on the possible location and mode of binding of these HQ derivatives. Except for the homoproline derivative, the amino acid conjugates were found to be weak inhibitors of these transporters.

1. Introduction

8-Hydroxyquinolines (HQ) are privileged structures in medicinal chemistry, including anticancer therapy, acting as potent and specific ligands for various biological targets. Their versatility arises from structural modifications of functional groups, complemented by favorable drug-like properties (DeSimone et al., 2004; Duarte et al., 2007). The targeting of multidrug resistant (MDR) cancer cells, which

* Corresponding authors.
E-mail addresses: domotor.o@chem.u-szeged.hu (O. Dömötör), borics.attila@brc.hu (A. Borics).

https://doi.org/10.1016/j.ejps.2025.107187
Received 20 March 2025; Received in revised form 10 June 2025; Accepted 27 June 2025
Available online 3 July 2025
0928-0987/© 2025 The Authors. Published by Elsevier B.V. This is an open access article under the CC BY-NC-ND license (http://creativecommons.org/licenses/by-nc-nd/4.0/).

developed resistance not only to the original drug used for the treatment, but also to structurally and mechanistically distinct drugs, has been associated with certain HQ-derived Mannich bases in our previous studies (Türk et al., 2009; Pape et al., 2021; Cserepes et al., 2020; Pape et al., 2022; Pape et al., 2018). In cancer, MDR often develops by the overexpression of P-glycoprotein (Pgp, ABCB1), and it is associated with the failure of chemotherapy. (Szakács et al., 2006; Dong et al., 2023). Paradoxically, MDR cells expressing Pgp exhibit an increased, rather than decreased sensitivity to certain HQs, referred to as MDR-selectivity (Türk et al., 2009; Füredi et al., 2017; Pape et al., 2018; Pape et al., 2021; Pape et al., 2022; Pivarcsik et al., 2023; Pivarcsik et al., 2024). Mechanistic studies on NSC297366, a HQ-derived MDR-selective Mannich base, have induced iron depletion in Pgp expressing MDR cells (upregulation of transferrin receptor protein 1 (TfR1) gene expression, increased levels of hypoxia inducible factor (HIF)-1α), which could be abrogated by the Pgp inhibitor tariquidar (TQ) (Cserepes et al., 2020). The decrease of intracellular iron and NSC297366 levels could be directly connected to Pgp activity by total-reflection X-ray fluorescence and HPLC-MS analyses. Pgp dependent iron depletion has also been demonstrated for related HQ structures (5-chloro-7-(piperidin-1-ylmethyl)quinolin-8-ol and the active form of NSC297366) (Pape et al., 2021).

Iron-complexation ability and acid–base properties are important factors modulating the MDR-selective anticancer effect of HQ-derived Mannich bases. In recent years we have conducted systematic structure–activity relationship analysis on numerous HQ-Mannich base derivatives (Pape et al., 2022; Pape et al., 2021; Pivarcsik et al., 2023; Pivarcsik et al., 2021; Mészáros et al., 2020; Dömötör et al., 2017). MDR-selective toxicity could be significantly enhanced by the introduction of halogens in position 5 on the HQ ring (R5) and a methylene-bridged amine at R7. The observed trends show a strong correlation with the proton dissociation constant (K_a) of the hydroxyl group. However, the potent HQ derivatives like NSC297366, suffer from poor water solubility, which reduces drug-likeness of the developed molecules. To overcome this obstacle, we have substituted the R7-methylen-amino moiety to yield proline (Pro) and homoproline (hPro) functions, and we also tested the Cl-to-NO_2 exchange in R5 position. These modifications resulted in zwitterions with remarkably increased water solubility, which, along with their various metal complexes, were characterized in previous publications (Mészáros et al., 2020; Pivarcsik et al., 2021; Pivarcsik et al., 2023). These molecules have retained a moderate MDR-selective cytotoxicity but lower overall toxicity, assuming unchanged mechanism, but decreased cell entry due to decreased lipophilicity.

The mechanism of action, proton dissociation, metal-complexation and lipophilicity are known for these compounds, while interaction with transport proteins in blood and cell membranes, influencing the pharmacokinetic behaviour of these molecules, are not yet discovered. As these amino acid conjugates are partly anionic at physiological pH, they can be substrates of the most abundant serum protein human serum albumin (HSA) and organic anion transporting polypeptides (OATPs) located in the cell membrane of various tissues. HSA acts as a carrier for several drugs due to its accumulation in tumors as a consequence of the enhanced permeability and retention effect (Elsadek and Kratz, 2012). A higher affinity for HSA results in a greater protein-bound drug fraction, which can significantly decrease the free drug concentrations and consequently extend the biological half-life or, in extreme cases, hinder the attainment of therapeutic drug levels in the blood (Elsadek and Kratz, 2012). Among the selected compounds quantitative data on their HSA binding are sparse (Pivarcsik et al., 2023).

OATPs are solute carrier-type organic anion transporters with numerous subfamilies. OATP1B1 plays an important role in hepatic uptake of drugs for clearance, inhibition or induction of this protein may be the underlying mechanism of clinically relevant drug-drug interactions (Schulte and Ho, 2019; Müller and Fromm, 2011). Recent findings have suggested that OATPs (*e.g.* OATP1B3 and OATP2B1) may have an important pathophysiological role in certain cancers (Svoboda et al., 2011; Kounnis et al., 2011). OATP2B1 is expressed in a variety of human tissues, mainly in enterocytes, determining intestinal absorption (Nozawa et al., 2004; Schulte and Ho, 2019). Therefore, identification of OATP substrates, especially the ones binding to OATP1B1 has become a critical aspect of early drug development and according to international (FDA, EMA) regulations, interaction between drug candidates and OATPs should be investigated. In our previous study $HQNO_2$-L-Pro showed weak inhibitory effect on the transport activity of OATP1B1 and OATP2B1 (Pivarcsik et al., 2023).

With the present study our aim was to explore how differences in structural and physicochemical properties affect HSA and OATP binding and whether they are cytotoxic to parental and MDR cancer cells, with MDR-selectivity. To this end it was essential to complete the solution-phase characterization (K_a values and *n*-octanol/water distribution coefficients (*D*)), inhibition on OATP1B1 and OATP2B1 transporters and binding to HSA under the same conditions for the selected four 8-hydroxyquinoline-derived Mannich bases along with the reference structures HQ, HQCl and $HQNO_2$ (Chart 1). Cytotoxic efficacy was studied on cocultured parental (MES-SA) and Pgp-expressing MDR (MES-SA/Dx5 and MES-SA/B1) cells. HSA binding was analysed by the combination of various techniques: UV–vis spectrophotometry, time-resolved and steady state fluorometry, circular dichroism (CD) spectroscopy, saturation transfer difference (STD) NMR and ultrafiltration. Inhibition on OATP1B1 and OATP2B1 transporters was assayed *in vitro*, and molecular docking was used to model binding of the HQ derivatives to the transporters.

2. Results and discussion

2.1. Anticancer activity of the investigated HQ compounds against parental and MDR cancer cells

Cytotoxicity tests were conducted for compounds in Chart 1 on cocultured cell lines. In a coculture, the parental MES-SA mCherry (mCh), its MDR counterparts MES-SA/Dx5 eGFP and Pgp-expressing MES-SA/B1 mOrange (mOr) cells are cultivated in the same well. In the triple-fluorescence-based cytotoxicity screen, the effect of a drug is monitored in parallel on three cell lines expressing different fluorescent proteins (mCh, eGFP, mOr) (Windt et al., 2019). The difference between MES-SA/Dx5 and MES-SA/B1 relies on the origin of Pgp expression, virally transfected B1 cells produce Pgp permanently, while in Dx5 cells Pgp expression is increased as a result of doxorubicin selection (Windt et al., 2019). The obtained IC_{50} values and selectivity ratios (SR) are shown in Tables 1 and 2 (see cell viability curves in Figure S1). SR is a measure of a compound's effectiveness against MDR cancer cells over parental cells, and can be expressed as quotient of IC_{50} against parental over IC_{50} on MDR (MES-SA/Dx5 or MES-SA/B1) cells. HQCl-L-Pro and HQCl-*D*-hPro displayed similar cytotoxicity on all the tested cell lines, while HQCl-D-Pro exhibited somewhat higher IC_{50} values. The compounds showed higher anticancer activity on the MDR cells, and their selectivity ratios were higher than those of the reference compounds (HQ, HQCl). MDR-selective cytotoxicity of the proline/homoproline derivatives in MES-SA/Dx5 cells was abrogated in the presence of the Pgp inhibitor tariquidar (TQ) practically to the effectivity obtained on parental MES-SA cells (Table 1). This finding suggests the critical contribution of this membrane efflux pump in the MDR-selective toxicity. $HQNO_2$-L-Pro showed much weaker cytotoxicity against all cell lines compared to the other amino acid conjugates, indicating that the exchange of the chlorine substituent to the nitro group had a strong effect on the anticancer activity of these Mannich bases. On the other hand, no significant differences were observed between the behavior of 5-chloro (HQCl) and 5-nitro ($HQNO_2$) reference compounds.

The HQ–amino acid conjugates were formerly tested against a chemosensitive human colon adenocarcinoma cell line (Colo205) and its doxorubicin-resistant counterpart (Colo320) (see Table S1) (Pivarcsik

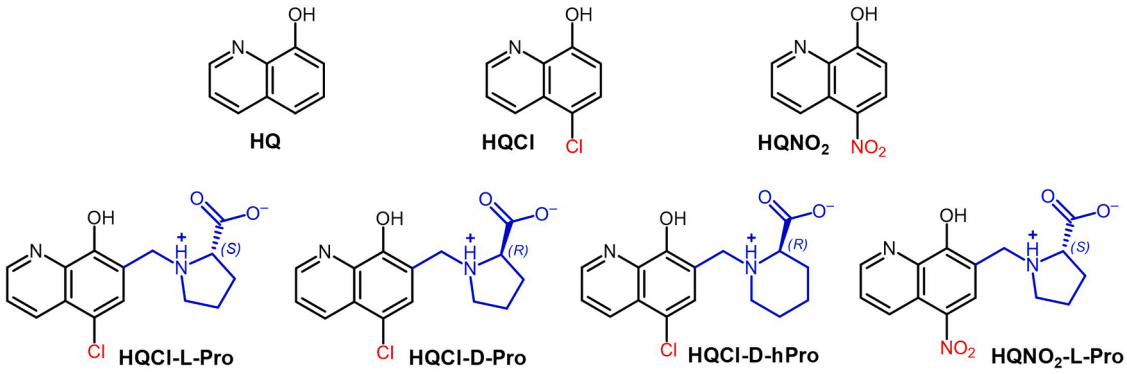

Chart 1. Chemical structures of the reference compounds (HQ, HQCl, $HQNO_2$) and 8-hydroxyquinoline-derived Mannich bases.

Table 1
In vitro cytotoxicity expressed as IC_{50} (μM) values of the compounds HQCl-L-Pro, HQCl-D-Pro, HQCl-D-hPro, $HQNO_2$-L-Pro in the coculture assay on parental MES-SA mCherry and the MDR MES-SA/Dx5 eGFP and MES-SA/B1 mOrange cell lines (144 h incubation time). Selected tests were also performed in the presence of the Pgp inhibitor tariquidar (TQ). Selectivity ratios (SR) were calculated as the ratio of the IC_{50} values obtained in parental and MDR cells.

	HQCl-L-Pro		HQCl-D-Pro		HQCl-D-hPro		$HQNO_2$-L-Pro	
	IC_{50} (μM)	(±)	IC_{50} (μM)	(±)	IC_{50} (μM)	(±)	IC_{50} (μM)	(±)
MES-SA	31.3[a]	9.9/7.5	73.6	9.8/8.6	35.4	7.5/6.2	217	29/26
MES-SA + TQ	29.5	2.9/2.7	64.1	4.0/3.7	28.8	6.4/5.2	227.3[b]	2.6/2.6
MES-SA/Dx5	5.6[a]	1.5/1.2	11.6	5.2/3.6	6.3	2.1/1.6	103[b]	30/23
MES-SA/Dx5 + TQ	26.3	4.0/3.5	63.1	2.8/2.7	23.3	5.2/4.3	229[b]	51/42
MES-SA/B1	18.4	4.5/3.6	55.0	4.3/4.0	30.5	5.3/4.5	162	14/13
Selectivity ratio (SR (*p*))								
MES-SA / MES-SA/Dx5	5.6[c]		6.4[c]		5.6[c]		2.1[c]	
MES-SA +TQ / MES-SA/Dx5 + TQ	1.1 [n.s.]		1.0 [n.s.]		1.2 [n.s.]		1.0 [n.s.]	
MES-SA / MES-SA/B1	1.7[c]		1.3[c]		1.2 [n.s.]		1.3[d]	

[a] IC_{50} values for the respective cell type assayed in monoculture: MES-SA: 23 μM, MES-SA/Dx5: 4.3 μM (Pivarcsik et al., 2023).
[b] IC_{50} values for the respective cell type assayed in monoculture: MES-SA: 226 μM, MES-SA + TQ: 223 μM, MES-SA/Dx5: 97 μM, MES-SA/Dx5 + TQ: 219 μM (Pivarcsik et al., 2023).
[c] $p < 0.01$.
[d] $p < 0.05$; n.s.: not significant.

et al., 2021; Mészáros et al., 2020; Pivarcsik et al., 2023). The trends of IC_{50} values observed on MES-SA, Colo205 and Colo320 cells are similar, although the concrete values are different. By comparing the citotoxicities obtained on mono, and cocultured parental or Dx5 cell lines, the IC_{50} values do not differ considerably (see data in legend of Tables 1 and 2, Pivarcsik et al., 2023, Dömötör et al., 2017). Since the actual charge and lipophilic character of the compounds may have a strong impact on the cellular uptake and the overall anticancer activity, the (de)protonation processes and the lipophilicity of these compounds are compared in the next chapter.

2.2. Proton dissociation processes and lipophilicity of the compounds

The actual protonation state, thus, the overall charge of a compound as well as certain physico-chemical properties, such as solubility and lipophilicity, have great importance in drug development due to the fact that all these parameters influence the pharmacokinetic (ADME) properties of a drug. Moreover, the ability to form intra- or intermolecular hydrogen bonds can greatly affect their interaction with biomolecules (*e.g.* receptors, transport proteins, enzymes). The proton dissociation processes and constants (K_a) of the reference compound HQ and the

Table 2
In vitro cytotoxicity expressed as IC_{50} (μM) values of the reference compounds HQ, HQCl and $HQNO_2$, and etoposide in the coculture assay on the parental MES-SA mCherry and the MDR MES-SA/Dx5 eGFP and MES-SA/B1 mOrange cell lines (144 h incubation time). Selectivity ratios (SR) were calculated as the ratio of the IC_{50} values obtained in parental and MDR cells.

	HQ		HQCl		$HQNO_2$		etoposide	
	IC_{50} (μM)	(±)	IC_{50} (μM)	(±)	IC_{50} (μM)	(±)	IC_{50} (μM)	(±)
MES-SA	2.5[a]	0.1/0.1	5.0	0.3/0.3	5.7	0.3/0.3	0.12	0.3/0.3
MES-SA/Dx5	1.39[a]	0.04/0.04	3.8	0.6/0.5	3.7	0.3/0.3	1.93	0.3/0.3
MES-SA/B1	2.5	0.1/0.1	5.2	0.1/0.1	5.4	0.2/0.2	1.10	0.2/0.2
Selectivity ratio (SR (*p*))								
MES-SA / MES-SA/Dx5	1.77[b]		1.34[c]		1.53[b]		0.06[b]	
MES-SA / MES-SA/B1	0.99 [n.s.]		0.98 [n.s.]		1.06 [n.s.]		0.11[b]	

[a] IC_{50} values for the respective cell type assayed in monoculture: MES-SA: 3.3 μM, MES-SA/Dx5: 1.08 μM in reference (Dömötör et al., 2017).
[b] $p < 0.01$.
[c] $p < 0.05$; n.s.: not significant.

HQ–Mannich bases have been reported in our previous works using various methods and ionic strengths (pH-potentiometry, UV-visible spectrophotometry and ^{1}H NMR spectroscopy; 0.2 M KCl, 0.2 M KNO_3, 0.1 M KCl (Mészáros et al., 2020; Pivarcsik et al., 2021; Pivarcsik et al., 2023; Enyedy et al., 2012). In the case of HQCl and $HQNO_2$, literature data are available on the pK_a values obtained at low ionic strength (0.01 M KCl) or at 0.1 M KCl, in the presence of < 1 % ethanol (Klofutar et al., 1975; Paljk et al., 1975). Only a rough pK_a estimation for HQCl at I = 0.2 M KNO_3 in water was reported previously (Mészáros et al., 2020), therefore we performed spectrophotometric measurements using long path length and more dilute conditions. The pK_a values for these two compounds were determined in water without precipitation (Table 3, see Figure S2 for the UV–vis titration of HQCl).

The fully protonated forms of the three reference molecules, HQ, HQCl and $HQNO_2$, can be characterized by two pK_a values belonging to the quinolinium nitrogen (N_qH^+) and the phenolic group (OH). Apparently, the negative inductive (–I) effect of the chloro substitution is not as significant on the pK_a values as the negative mesomeric (–M) and –I effects of the nitro substituent. The proton dissociation constants determined in this work correspond well to literature data (Klofutar et al., 1975; Paljk et al., 1975). Meanwhile, the fully protonated forms of the HQ–amino acid conjugates (HQCl-L-Pro, HQCl-D-Pro, HQCl-D-hPro, $HQNO_2$-L-Pro, Chart 1) have two additional dissociative moieties (COOH and $N_{Pro/hPro}H^+$). In these molecules the carboxylic group (COOH) becomes deprotonated at pH>2, while the tertiary ammonium group ($N_{Pro/hPro}H^+$) remains protonated over a wide pH range and starts to deprotonate only at pH>10. As a consequence, the (homo)proline moiety retains a zwitterionic character in a wide pH range (2 − 10). The pK_a values of $N_qH^+$and OH are lower compared to those of the reference structures HQCl and $HQNO_2$. For a better understanding of the actual charge status of the compounds, speciation at pH = 7.4 (pH of blood), 5.5 (a slightly acidic pH, such as the decreased extracellular pH found in the tumor microenvironment) and pH 2.1 (a typical gastric pH) are computed and presented in Tables 3 and 4. At pH 7.4, the majority of HQ and HQCl are neutral, while $HQNO_2$ is mostly negatively charged. By decreasing the pH from 7.4 to 2.1, positively charged species (H_2L^+) become predominant for these three compounds. $HQNO_2$-L-Pro is found in its monoanionic form (HL^-) at pH 7.4, while in the case of the 5-chloro-(h)Pro derivatives the fraction of neutral and anionic forms are comparable. Formation of an intramolecular hydrogen bond was suggested between the protonated (homo)proline NH^+ and the phenolate oxygen of these HQ–amino acid conjugates (Pivarcsik et al., 2021). The molecules have excellent aqueous solubility at pH 7.4 (Pro derivatives: $S_{7.4}$ > 10 mM, HQCl-D-hPro: $S_{7.4}$ ~5 mM) (Pivarcsik et al., 2023; Pivarcsik et al., 2021; Mészáros et al., 2020). At pH 5.5, $HQNO_2$-L-Pro is almost in equal quantities in HL^- and H_2L^0, and the 5-chloro derivatives are present almost exclusively as H_2L^0. At strongly acidic conditions (pH 2.1) positively charged forms (H_3L^+ and H_4L^{2+}) are dominant for these HQ–amino acid conjugates, however the exact protonation state of the molecules cannot be established with full certainty due to the limiting pK_a(COOH) values.

Distribution coefficients (D) characterizing lipophilicity were determined via traditional n-octanol/water partitioning at pH 7.4, 5.5 and 2.1. HQ is highly lipophilic at pH 7.4. More positively charged species (H_2L^+) are present in the solution by decreasing the pH, and as a result, log$D$ values become lower. For HQCl and $HQNO_2$, the lipohilicity – pH profile is slightly different, but they are definitely lipophilic at the studied pH values. The HQ–amino acid conjugates are generally more hydrophilic at the tested pH values owing to their zwitterionic structure, $HQNO_2$-L-Pro is definitely hydrophilic.

Table 3
Proton dissociation constants (pK_a) of the investigated reference compounds and their structure in the fully protonated form, the calculated fractions of the species in different protonation states (%) and distribution coefficients (D) at pH = 7.4, 5.5 and 2.1 {t = 25 °C; I = 0.1 M KCl}.

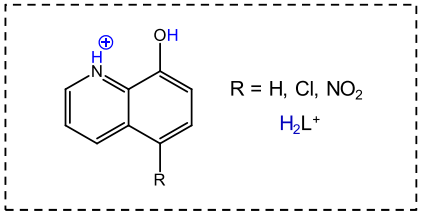

	HQ	HQCl	$HQNO_2$
pK_a (N_qH^+)	4.99[a]	3.82 ± 0.03[b,c,d]	2.56 ± 0.03[c,d]
pK_a (OH)	9.51[a]	9.13 ± 0.05[b,c,d]	6.13 ± 0.03[c,d]
species at pH = 7.4	HL^0: 99 % L^-: 1 %	HL^0: 98 % L^-: 2 %	HL^0: 5 % L^-: 95 %
species at pH = 5.5	H_2L^+: 24 % HL^0: 76 % L^-: 0 %	H_2L^+: 2 % HL^0: 98 % L^-: 0 %	H_2L^+: 0 % HL^0: 81 % L^-: 19 %
species at pH = 2.1	H_2L^+: 100 % HL^0: 0 %	H_2L^+: 98 % HL^0: 2 %	H_2L^+: 74 % HL^0: 26 %
log$D_{7.4}$	+1.81[e]	+1.93 ± 0.07	+1.46 ± 0.04
log$D_{5.5}$	+1.70 ± 0.08	+2.41 ± 0.23	+1.87 ± 0.04
log$D_{2.1}$	−0.84 ± 0.05	+1.11 ± 0.04	+1.34 ± 0.02

[a] I = 0.20 M (KCl), data taken from ref. (Enyedy et al., 2012).
[b] pK_a (N_qH^+) = 3.75 ± 0.03, pK_a (OH) = 9.19 ± 0.04 in I = 0.20 M (KNO_3), former estimation in I = 0.2 M KNO_3: pK_a (N_qH^+) = 3.8, pK_a (OH) = 7.6 (Mészáros et al., 2020).
[c] HQCl: pK_{a1} = 3.79, pK_{a2} = 9.29; $HQNO_2$: pK_{a1} = 2.51, pK_{a2} = 6.36 in I = 0.01 M, <1 % (v/v) ethanol/water, data taken from ref. (Klofutar et al., 1975).
[d] HQCl: pK_{a1} = 3.84, pK_{a2} = 9.29; $HQNO_2$: pK_{a1} = 2.69, pK_{a2} = 6.31 in I = 0.1 M, <1 % (v/v) ethanol/water, data taken from ref. (Paljk et al., 1975).
[e] Data taken from ref. (Dömötör et al., 2017).

Table 4
Proton dissociation constants (pK_a) of the investigated conjugates, the general structure in the fully protonated form, the calculated fractions of the species in different protonation states (%) and distribution coefficients (D) at pH = 7.4, 5.5 and 2.1 {t = 25 °C; I = 0.1 M KCl}.

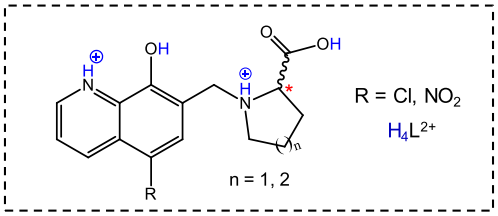

	HQCl-L-Pro	HQCl-D-Pro	HQCl-D-hPro	$HQNO_2$-L-Pro
pK_a (COOH)	<2[a]	<2[b]	<2[b]	<2[c]
pK_a (N_qH^+)	2.22[a]	2.13[b]	2.43[b]	<2[c]
pK_a (OH)	7.63[a]	7.77[b]	7.49[b]	5.43[c]
pK_a ($N_{hPro/ProH}^+$)	>11[a]	>11[b]	11.43[b]	10.75[c]
species at pH = 7.4	$H_2L^{0\,(+/-)}$: 63 % $HL^{-\,(+/2-)}$: 37 %	$H_2L^{0\,(+/-)}$: 70 % $HL^{-\,(+/2-)}$: 30 %	$H_2L^{0\,(+/-)}$: 55 % $HL^{-\,(+/2-)}$: 45 %	$H_2L^{0\,(+/-)}$: 1 % $HL^{-\,(+/2-)}$: 99 %
species at pH = 5.5	$H_2L^{0\,(+/-)}$: 99 % $HL^{-\,(+/2-)}$: 1 %	$H_2L^{0\,(+/-)}$: 99 % $HL^{-\,(+/2-)}$: 1 %	$H_2L^{0\,(+/-)}$: 99 % $HL^{-\,(+/2-)}$: 1 %	$H_2L^{0\,(+/-)}$: 46 % $HL^{-\,(+/2-)}$: 54 %
log$D_{7.4}$	−0.02[a]	−0.02[b]	+0.36[b]	−0.94[c]
log$D_{5.5}$	+0.07 ± 0.02	+0.09 ± 0.02	+0.44 ± 0.03	−0.91[c]
log$D_{2.1}$	−0.28 ± 0.02	−0.28 ± 0.03	−0.11 ± 0.04	−1.59 ± 0.02

[a] Data taken from ref. (Mészáros et al., 2020).
[b] Data taken from ref. (Pivarcsik et al., 2021).
[c] pK_a (OH) = 5.50, pK_a ($N_{Pro}H^+$) = 10.78 in I = 0.20 M (KNO_3), data taken from ref. (Pivarcsik et al., 2023).

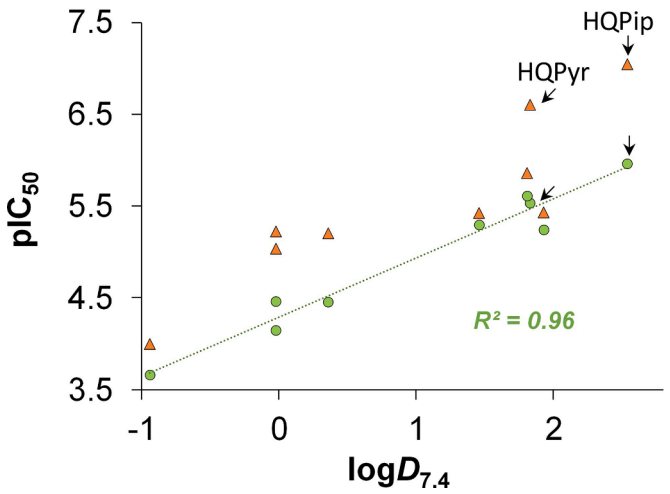

Fig. 1. Negative decadic logarithm of the cytotoxicity (pIC_{50}) values determined on MES-SA (●) and MES-SA/Dx5 (▲) cells as a function of lipophilicity ($logD_{7.4}$) for compounds HQ, HQCl, $HQNO_2$, HQCl-L-Pro, HQCl-D-Pro, HQCl-D-hPro and $HQNO_2$-L-Pro. Data obtained for structurally related compounds including 5-chloro-7-(pyrrolidin-1-ylmethyl)quinolin-8-ol (HQCl-pyr) and 7-(1-piperidinylmethyl)-8-hydroxyquinoline) (HQCl-pip) are also included (Pivarcsik et al., 2024).

By examining the cytotoxicity values obtained against parental MES-SA, Colo205 and doxorubicin resistant Colo320 cells, a broadly linear relationship is found between the negative decadic logarithm of the IC_{50} (pIC_{50}) values and the $logD_{7.4}$ values of the compounds (Fig. 1 and S3). Data obtained for related compounds (5-chloro-7-(pyrrolidin-1-ylmethyl)quinolin-8-ol and 5-chloro-7-(piperidin-1-ylmethyl)quinolin-8-ol) are also included in the data set (Pivarcsik et al., 2024). This correlation suggests that passive uptake is the most likely route of these molecules to enter cancer cells. In the MES-SA/Dx5 cell line the correlation is poor, as cytotoxicity is influenced by other factors related to functional ABCB1 (Fig. 1).

2.3. Binding to human serum albumin

The albumin binding of the compounds was studied by the combination of spectroscopic techniques (UV–vis, fluorometry, circular dichroism and STD NMR spectroscopies) and ultrafiltration. As shown in Fig. 2 (and Figure S4), the compounds displayed spectral changes to varying extents in the presence of HSA. By a closer look at the absorption spectra of $HQNO_2$ in Fig. 2b, the initial isosbestic point at 435 nm shifts to 445 nm at higher protein concentrations. The absorbance changes at the chosen wavelengths also refer to the binding of more than one ligand per albumin. Thus, two stepwise binding constants, $logK'_1 = 5.6 \pm 0.1$ and $logK'_2 = 4.4 \pm 0.1$, could be computed with HypSpec software (Gans et al., 1996). Calculated and experimental data give a good fit in Fig. 2c. For HQCl, neither the one-site nor the two-site model calculations yielded satisfactory results, although the binding of at least two molecules per albumin is evident (Figure S4). Moderate spectral variation was observed for HQ and the HQCl-*L/D*-Pro derivatives, while the spectrum of $HQNO_2$-L-Pro was barely affected by the addition of HSA (Figure S4). It is important to note that this phenomenon, however, does not mean an unequivocal lack of binding and a smaller spectral change alone does not mean weaker binding to the protein. The absorbance changes for HQCl-D-Pro, HQCl-L-Pro and HQCl-D-hPro suggest also the binding of more than one molecule per albumin (Figure S4), but spectral data could not be fitted well for one binding site and the two-site model resulted in highly uncertain stepwise binding constants.

According to the ultrafiltration studies, multiple binding sites are available for HQCl, $HQNO_2$ and HQCl-D-hPro on HSA, as >50 % of these molecules could bind to 0.5 equivalent of albumin (Fig. 3a). The other compounds, HQ, HQCl-*L/D*-Pro and $HQNO_2$-L-Pro, bind with lower affinity to HSA. The two weakest binders are HQCl-L-Pro and $HQNO_2$-L-Pro. Studies conducted with human blood serum (diluted approximately to the corresponding HSA-to-compound ratios) underlines the prominent role of albumin in the blood transport of these molecules, since similar binding patterns to albumin were obtained. In the case of $HQNO_2$, albumin binding was studied in more detail at various HSA-to-compound ratios. The two-site model provided also a better fit here (Fig. 3b). At the same time the binding of more than two $HQNO_2$ molecules per HSA cannot be excluded.

Circular dichroism spectra were recorded and analyzed from both perspectives: the protein's structural changes and the influence of the binding on the intrinsic bands of the Mannich bases containing a chiral amino acid side chain. The addition of HQ and its derivatives applied in 37–50-fold excess (see example for HQCl-D-Pro and $HQNO_2$-L-Pro in Figs. 4a and S5, respectively) did not affect the CD spectrum of native HSA. These results indicate that, as expected, the binding of the compounds do not affect the overall structure of HSA. At the same time, addition of HSA induced a significant gradual increase of a negative band in the CD spectra of the D-Pro or D-hPro substituted HQCl derivatives (Fig. 4b), whereas CD spectra of $HQNO_2$-L-Pro were less affected by the addition of HSA.

STD NMR spectroscopy was used to map the key moieties of the HQ molecules responsible for albumin binding. This technique exploits the exchange process between the protein-bound and free levels of a weak binding ligand. As strong binding molecules, $HQNO_2$ and HQCl could not be analyzed by STD spectroscopy, since this method is more suitable for weakly or moderately binding ligands. The other molecules showed different binding patterns, which is most easily represented by relative STD amplification values, shown in Fig. 5 (see spectra in Figure S6 and calculation in the Experimental Section), where higher percentage values reflect closer relative proximity of that hydrogen to the binding site. The STD amplification patterns of the respective C**H** groups is very similar for HQCl-D-Pro and HQCl-D-hPro, while the L-Pro derivatives display different patterns, namely *D* and *L* derivatives bind in different orientation to albumin. Quantitative evaluation (calculation of K_D values) of the measurements was not performed, as we assume the

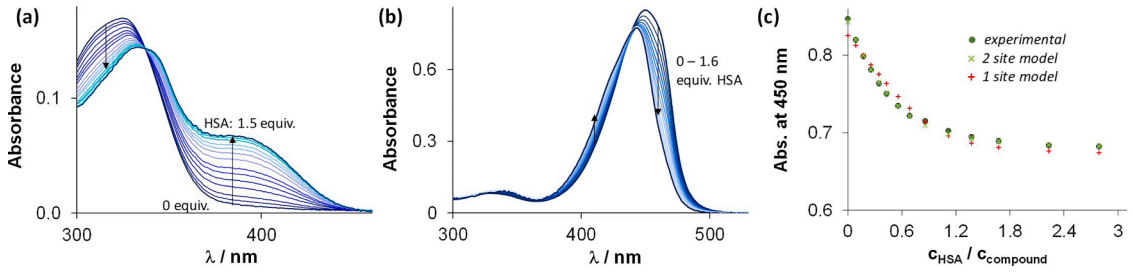

Fig. 2. UV–vis absorption spectra of (a) HQCl and (b) $HQNO_2$ in the presence of increasing HSA concentrations and (c) the experimental and the fitted absorbance values of the $HQNO_2$–HSA system at 450 nm with one and two binding site models. {$c_{comp} = 65$ μM (a), 27 μM (b); $\ell = 1$ cm; $t = 25$ °C; pH = 7.4 (PBS')} *Note: one-site model:* $logK' = 5.8 \pm 0.1$; *two-site model:* $logK'_1 = 5.6 \pm 0.1$, $logK'_2 = 4.4 \pm 0.1$.

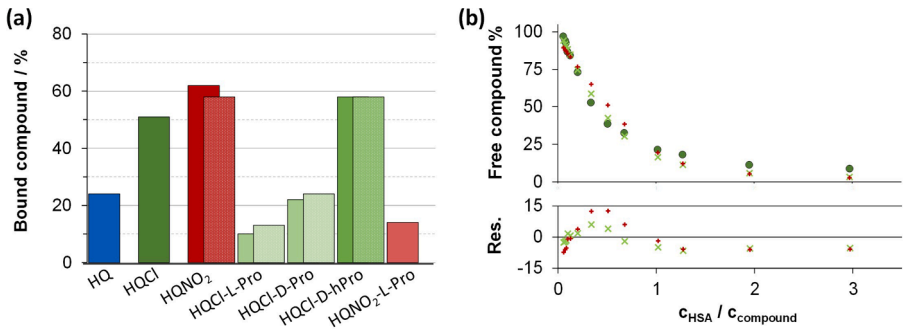

Fig. 3. (a) Bar chart of the bound compound fractions obtained in ultrafiltration – UV–vis studies in the indicated HSA – compound 1:2 (filled bars) and diluted human serum – compound (dotted bars) systems. (b) Experimental (●) and fitted data points for the ratio of the free compound (%) according to the one-site (+) and two-site (×) models in the HSA – $HQNO_2$ system obtained in UV–vis titration experiment. Residuals (Res.) show the difference between the point pairs. {c_{comp} = 50 or 100 μM (a), 40 μM (b); human serum diluted to approximately reach the corresponding HSA-to-compound ratios; t = 25 °C; pH = 7.4 (PBS')}.

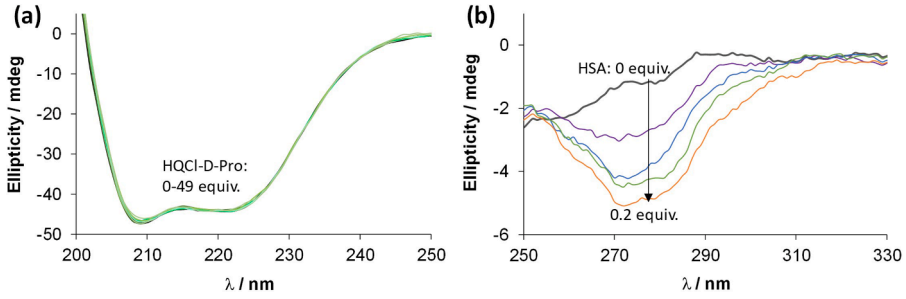

Fig. 4. Circular dichroism spectra of (a) HSA titrated by HQCl-D-Pro and (b) HQCl-D-Pro titrated by HSA {(a): c_{HSA} = 2.1 μM, ℓ = 2 mm; (b): c_{comp} = 98 μM, ℓ = 1 cm; t = 25 °C; pH = 7.4 (PBS')}.

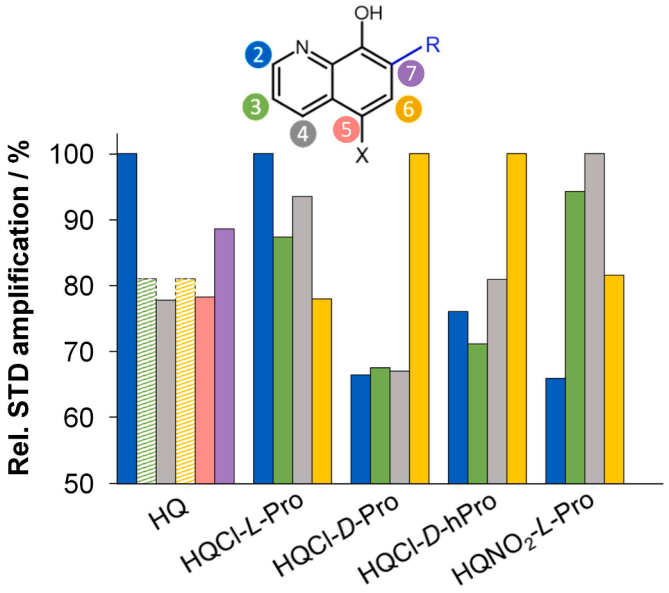

Fig. 5. Relative STD amplification of the respective hydroxyquinoline C**H** peaks of the listed molecules in the presence of 0.1 equivalent of HSA. Striped bars of HQ represent an average for the overlapping C$\mathbf{H}^3$ and C$\mathbf{H}^6$ signals. {c_{comp} = 100 μM, t = 7 °C; pH = 7.4 (PBS', 10 % (v/v) D_2O).

presence of more than one binding site for these compounds in HSA based on the UV–vis and ultrafiltration experiments.

Next, spectrofluorometric studies were performed, to obtain information on the site-specificity of the binding process. Of note, the studied HQ derivatives have negligible fluorescence at pH 7.4 in PBS' buffer, however, moderate fluorescence may be observed due to the formation of complexes with trace metal contaminants (Mg(II), Ca(II), Zn(II), Al(III), *etc.*), which are fluorogenic and the presence of even tiny amounts of metal complexes can cause interfering fluorescence (see more details in Figure S7 (Enyedy et al., 2012; Dömötör et al., 2013; Lytle et al. 1973)). To avoid this phenomenon, the use of 2 mM EDTA is recommended, which has been shown to have no effect on the binding of these substances to albumin. In the albumin quenching experiments, we followed the fluorescence of Trp^{214} situated near to site I in HSA to monitor the binding to the protein. As shown in Fig. 6, addition of HQCl gradually quenches the fluorescence of Trp^{214}, leading to complete quenching by the addition of ~70 equiv. compound. The quenching curves in Fig. 6b decrease steeply for HQCl, $HQNO_2$ and HQCl-D-hPro. HQCl-*D/L*-Pro and $HQNO_2$-L-Pro quench the Trp^{214} fluorescence less effectively, and HQ seems to be the 'weakest' quencher. It should be clarified here that the intensity at which the quenching curves saturate does not necessarily correspond to the binding strength, which is more likely influenced by the distance between the fluorophore (Trp^{214}) and the bound small molecule, as well as the mode of interaction between them (Valeur 2001).

The binding strength of the compounds was characterized by the quenching constants (logK'_Q) listed in Table 5. The quenching constants show the following order: $HQNO_2$ > HQCl >> HQCl-D-hPro >> HQCl-D-Pro ≈ HQ ≈ HQCl-L-Pro ≈ $HQNO_2$-L-Pro. The quenching constant of $HQNO_2$ indicates strong binding to albumin, surpassing the binding strength of warfarin (logK' = 5.58), an anticoagulant drug that is 99 % bound to HSA in blood. (Dömötör et al., 2013; Bristol-Myers Squibb Canada, 2018). Individual spectra of HSA and the forming HSA-compound adducts were also calculated, and the relative intensities are shown in Table 5 at the emission maximum of HSA. The HSA adducts of HQCl, $HQNO_2$, HQCl-D-Pro and HQCl-D-hPro are practically non-fluorescent (see also Fig. 6a), while the adducts of L-Pro derivatives and HQ are fluorescent.

It is worth investigating the possible mechanism of the quenching

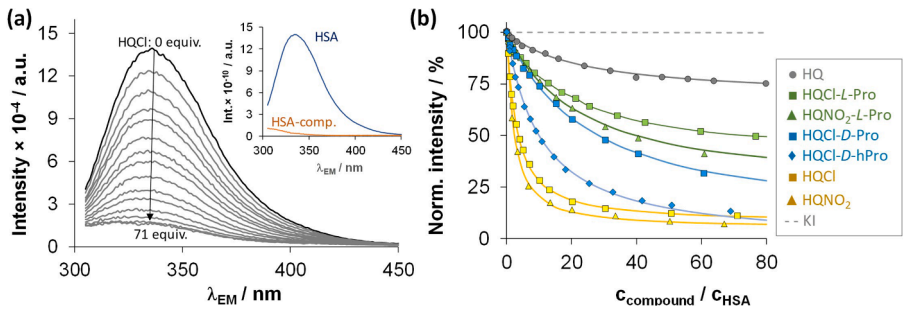

Fig. 6. (a) Fluorescence spectra obtained by the titration of HSA with HQCl. The inserted figure shows the individual spectra of HSA and compound-bound HSA. (b) Quenching curves at 340 nm for the indicated HQ-derivatives and potassium iodide (KI), the solid lines are the fitted titration curves {$c_{HSA} = 1$ μM, $\lambda_{EX} = 295$ nm; $t = 25$ °C, PBS'}.

Table 5
Fluorescence quenching constants (K_Q') and relative individual intensities of the forming HSA–compound adducts, and displacement constants (K'_{marker}) calculated for the HSA – WF / HSA – DG – HQ compound systems {$t = 25$ °C, PBS', 2 mM EDTA}.

compound	logK'_Q ± SD	relative individual intensity of the HSA adduct[a]	logK'_{WF} ± SD[b]	logK'_{DG} ± SD[c]
HQ	4.5 ± 0.1	62 %	< 4.0[d]	< 4.0[d]
HQCl	5.5 ± 0.1	3 %	5.0 ± 0.1	4.4 ± 0.1
$HQNO_2$	5.8 ± 0.1	5 %	5.8 ± 0.1	5.8 ± 0.1
HQCl-L-Pro	4.5 ± 0.1	27 %	< 4.0[d]	< 4.0[d]
HQCl-D-Pro	4.6 ± 0.1	0 %	4.5 ± 0.1	4.3 ± 0.1
HQCl-D-hPro	5.0 ± 0.1	0 %	4.7 ± 0.1	4.5 ± 0.1
$HQNO_2$-L-Pro	4.4 ± 0.2[e]	18 %	4.5 ± 0.1	4.2 ± 0.1[f]

[a] Relative intensities calculated at $\lambda_{EX} = 295$ nm and $\lambda_{EM} = 335$ nm with the formula: $I_{MOL(HSA\text{-}compound)} / I_{MOL(HSA)} \times 100$, where I_{MOL} = molar (individual) intensities of the respective species calculated with HypSpec (Gans et al., 1996).
[b] logK'(HSA-WF) = 5.58 (Dömötör et al. 2013).
[c] logK'(HSA-DG) = 5.24 (Dömötör et al. 2013); justification for this limit is given in Section S3.
[d] logK'_Q = 4.78 in PBS' (Pivarcsik et al., 2023).
[e] logK'_{DG} = 4.47 (Pivarcsik et al., 2023).

event; therefore, fluorescence lifetime measurements were also performed. HSA displays a two-exponential decay ($\tau_1 = 2.5 \pm 0.1$ ns ($\alpha_1 =$ 37 %), τ_2=7.0 ± 0.1 ns ($\alpha_2 = 63$ %)) that agrees well with literature data (Chadborn et al., 1999). By the addition of 13 equiv. HQCl-D-Pro, τ_1 (1.74 ± 0.1 ns) and τ_2 (5.94 ± 0.1 ns) values were reduced considerably. 4 equiv. HQCl resulted in a similar decrease of the lifetime of Trp^{214}. Although to a lesser extent, HQCl-L-Pro also reduced Trp^{214} lifetime values (see Table S2). This phenomenon is often explained by the collisional (dynamic) quenching mechanism of Trp. In our opinion, this is an oversimplified concept because potassium iodide (KI), a typical collisional quencher of HSA (Lakowicz, 2006; Chadborn et al., 1999) does not result in any decrease in HSA fluorescence applied in the same concentration range as the HQ compounds (Fig. 6b dashed line and Figure S8). Dilute conditions do not favor collisional relaxation mechanism. Instead, (fluorescence) resonance energy transfer (RET, FRET) is more likely to occur between the donor (Trp^{214}) and the acceptor (HQ derivative) molecule. The spectral overlap between the emission spectrum of HSA and absorption spectrum of the respective HQ derivatives, which is a prerequisite of RET, is significant and rather similar for the species, except HQ where the overlap integral is only 41 % in contrast to the other compounds (90–99 %, see Figure S9). Overlap integral values correlate well with the relative individual intensities of the species-bound HSA for the most compounds. A spectral overlap over 90 % is accompanied by practically total quenching of Trp^{214}. Deviation of HQCl-L-Pro from this correlation indicates that this molecule may orient in the binding site in a different way compared to the D-congener.

Fluorescent site marker displacement assays conducted with site markers for site I (warfarin, WF), site II (dansylglycine, DG) and site III (site IB, bilibrubin, BR) allow some more insight into the binding mode of these molecules. Besides the steady-state titrations, fluorescence decay of the respective systems was also monitored by time correlated single photon counting (TCSPC) technique. The fluorescence in a HSA – site marker system can be reduced by a third compound via (i) real competition at the respective site, (ii) interfering the environment of the site without displacing bound marker (allosteric effect) or alternatively by (iii) adduct formation between the free marker and the compound. Indicated lifetime (τ) and amplitude (α) values correspond to the nature (quality) and the quantity of each fluorophore presented in the system, respectively. In Fig. 7, the HSA – DG (1:1) system was titrated by $HQNO_2$, spectral changes indicate the effective displacement of DG from the albumin binding site. Lifetime measurements revealed a slightly more nuanced picture. The displacement of HSA-bound DG is well demonstrated by the decreasing amplitude of the HSA-bound DG (α_2) in Fig. 7b, but also the lifetime of the bound form (τ_2) decreases moderately upon the addition of $HQNO_2$. The latter phenomenon is most probably due to the parallel binding of $HQNO_2$ at (an)other site(s) slightly altering the environment of bound DG. A combination of cases (i) and (ii) occurs, while the adduct formation with free DG (iii) was excluded in independent measurements. In the case of the other HQ derivatives, the alteration of τ_2 is not typical, only the amplitudes change in favor of free DG, simple displacement reactions occur (see examples in Figure S10).

In the HSA – WF system, the emission maximum of the free WF hardly differs from that of the bound form (Fig. 8), differing only in intensity, making it more difficult to determine whether true displacement takes place when HQ compounds are added to the system. Additionally, lifetime data are somewhat more difficult to interpret: free WF is very short lived ($\tau_1 \approx 0.3$ ns), and there are two proven lifetime components ($\tau_2 \approx 1.4$ ns and $\tau_3 \approx 3.3$ ns) for bound WF (Karlsson et al., 2007; Nicholls et al., 2010). Due to the large number of parameters to be fitted, decay curves were recorded over a wider wavelength range, and decay associated spectra (DAS) were calculated by fitting them globally in the case of the HSA – WF – $HQNO_2$ ternary system. DAS in Figs. 8b–d

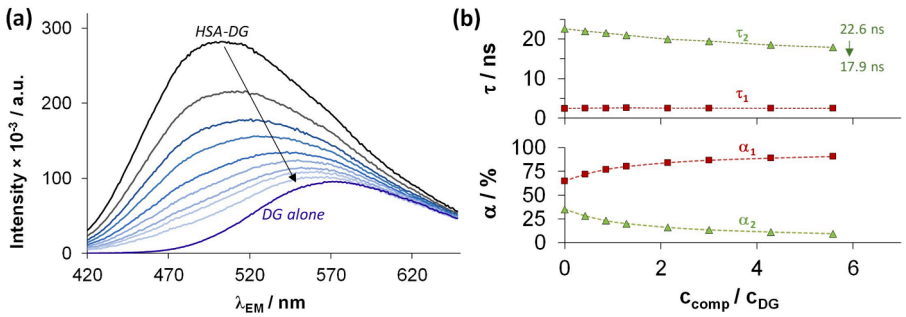

Fig. 7. (a) Fluorescence spectra of the HSA – DG (1:1) system titrated by $HQNO_2$ together with the fluorescence spectrum of free DG (a). (b) Fluorescence decay parameters calculated for the same system: lifetimes (τ_{1-2}) and amplitude (α_{1-2}) values, $\chi^2 \leq 1.13$. {$c_{HSA} = 5$ μM; $c_{DG} = 5$ μM; $\lambda_{EX} = 335$ nm (a) 360 nm (b), $\lambda_{EM} = 540$ nm (b); $t = 25$ °C; PBS'} (see details on the calculations in the Experimental section).

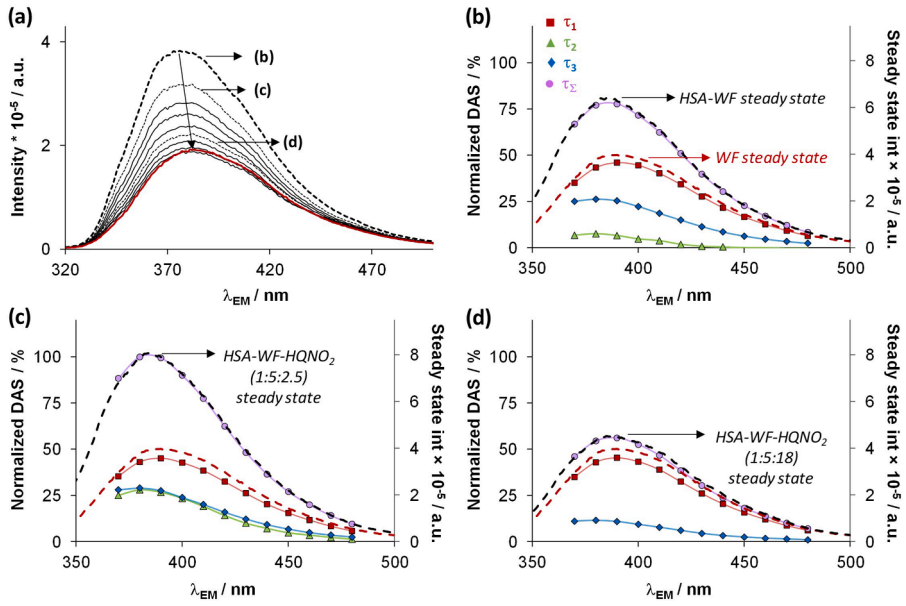

Fig. 8. (a): Steady state fluorescence spectra of the HSA – WF binary system titrated by $HQNO_2$. (b,c,d): Normalized decay-associated spectra (τ_{1-3}) and their sum (τ_Σ) deconvoluted from the decay curves recorded between λ_{EM} 370–480 nm for the systems HSA – WF (b) and HSA – WF – $HQNO_2$ 1:5:2.5 (c) 1:5:18 (d). Steady-state emission spectra of the respective systems (black dashed spectrum) and WF alone (red dashed spectrum) are depicted as well. Deconvoluted spectra belong to: free WF (■: $\tau_1 = 0.27$ ns); bound WF forms (▲: $\tau_2 = 1.44$ ns (b), 1.27 ns (c); ◆: $\tau_3 = 3.28$ ns (b), 2.69 ns (c), 2.63 ns (d)) and the sum of them (●). {$c_{HSA} = 1$ μM; $c_{WF} = 5$ μM; $c_{compound} = 0$ μM (b), 2.5 μM (c) or 5 μM (d); $\chi^2 = 1.10$ (b), 1.07 (c), 1.19 (d); $\lambda_{EX} = 300$ nm; $t = 25$ °C; in PBS'} (see details on the calculations in Section S4 of the Supplementary Material.).

show the spectral contribution of each fluorescent component to the total fluorescence of the studied systems. The scales of steady-state and DAS intensities were aligned to each other; hence the DAS of free WF (red ▲) represents the free fractions of WF. The trend in Figs. 8b–d shows that by the addition of $HQNO_2$ the fluorescence of the bound forms becomes minimal, the fluorescence of free WF increases, and approaches the spectrum of 5 μM WF (dashed red spectrum). Based on the τ parameters (see figure legends) both τ_2 and τ_3 decreased. A very similar picture to the HSA – DG – $HQNO_2$ ternary system applies, with alteration of the binding site and replacement of bound WF. HQCl caused similar changes in the HSA – WF system, while in the case of HQCl-L-Pro, there is no considerable change in these parameters even at high excess of the compound (Figures S11 and S12).

None of the HQ compounds could displace BR effectively, only HQCl-D-Pro decreased slightly the fluorescence of the HSA – BR system (Figure S13), however UV–vis measurements on the same system did not support the displacement of BR. The binding of these compounds at site IB is therefore not feasible.

Binding constants for site I and II were calculated with HypSpec, and are listed in Table 5 (Gans et al., 1996). The trend of the quenching and binding constants at site I show similarities to each other. In general, $\log K'_{WF}$ values are smaller than the quenching constants, which means that they are not compatible with each other, although WF binds in site I and the Trp^{214} resides also here. The presumed existence of multiple binding sites, and sensitivity of Trp^{214} for more distant binding can result in that discrepancy. Moreover, the constant from WF displacement is overestimated for $HQNO_2$ and HQCl, since, according to the lifetime experiments, not a simple marker displacement reaction takes place. A great difference applies between $\log K'_{DG}$ of $HQNO_2$ and the other compounds, however the constant for $HQNO_2$ is overestimated due to the same reason as mentioned above for $\log K'_{WF}$.

The literature data on the HSA binding of HQ compounds are limited, only one study is available on the interaction with $HQNO_2$ (Zhang et al., 2014). The authors found a quenching constant $K_Q' = 3.836 \times 10^5$ ($\log K_Q' = 5.58$), and the similarity with our results is reasonable, taking into account the different conditions ($\lambda_{EX} = 280$ nm) and mode of calculation (Stern-Volmer linearization) applied. UV–vis spectral changes reported for $HQNO_2$ upon addition of HSA are also similar to our observations. Formerly we have found weak binding of HQ on HSA based on fluorometric and UV–vis measurements, but have not

quantified the interaction (Enyedy et al., 2015; Dömötör et al., 2022). ^{1}H NMR studies also confirmed the binding of HQ and HQCl-L-Pro on HSA (Dömötör et al., 2021). Fluorescence quenching and DG displacement constants for $HQNO_2$-L-Pro was determined in our former work without the addition of EDTA ($\log K'_Q = 4.78$; $\log K'_{DG} = 4.47$) (Pivarcsik et al., 2023).

The more detailed results of the present study indicate at least two binding sites available for $HQNO_2$, HQCl, HQCl-*D*/*L*-Pro and HQCl-D-hPro. Fluorometric studies support the binding of all compounds at sites I and II with varying affinity. The strongest overall binding was found for $HQNO_2$, HQCl-D-hPro and HQCl. Quenching constants and binding constants calculated for site I support this trend. Binding strengths at site II are apparently lower than at site I, except for $HQNO_2$. The studied molecules are not able to displace BR from site IB (site III). Fluorescence lifetime measurements indicate that the displacement constants calculated from steady-state measurements for $HQNO_2$ are in fact overestimated, and the same is true for HQCl in the WF displacement experiment. Taken together, the ultrafiltration data show strong binding of these two compounds to HSA. For $HQNO_2$, stepwise binding constants, determined in UV–vis measurements, allow prediction of the HSA-bound fraction of the molecule at physiologically relevant concentrations. Based on our data 99.6 % of $HQNO_2$ is expected to be HSA-bound in a hypothetical system containing 630 μM HSA and 10 μM $HQNO_2$. This percentage is barely affected (99.5 %) when 100 μM $HQNO_2$ is applied, and is comparable to that of reported for WF (99 %) (Bristol-Myers Squibb Canada, 2018). Such predictions are not applicable using the binding constants determined by fluorometry, as they characterize the affinity for a given binding site but not directly the overall binding. However, an estimation was done for a molecule of single binding site ($\log K' = 4.4$; lowest quenching constant, calculated for $HQNO_2$-L-Pro) with the above conditions and 94–93 % is predicted to be HSA-bound. In all, these molecules can bind to HSA to a large or even extreme extent.

Another important insight is that quenching occurs through a RET mechanism. The studied molecules cannot displace BR from site IB (site III). An interesting difference applies between the binding affinities of the two enantiomers of HQCl-Pro: the D-enantiomer binds stronger to HSA than the L-isomer. By taking a look at the charge status of the compounds at pH 7.4 there is no clear correlation with the albumin binding affinities. In fact, Mannich bases are zwitterionic, while the reference compounds are not. The $\log D_{7.4}$ values show a weak correlation with binding data (Fig. 9), the correlation is better for the quenching constants compared to the results of ultrafiltration. The low albumin affinity of HQ is the most extreme outlier; drawing attention to the role of electron withdrawing group at the R5 position in albumin binding. This observation, however, should be confirmed by involving further derivatives in future studies.

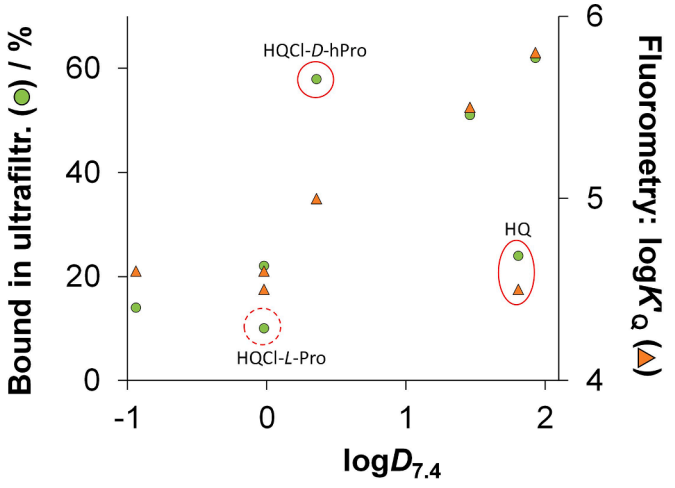

Fig. 9. HSA-bound fractions determined in ultrafiltration studies (●) and Trp^{214} quenching constants ($\log K'_Q$, ▲) as a function of lipophilicity ($\log D_{7.4}$) at pH = 7.4; mismatched points are indicated with red circles.

2.4. *In vitro inhibitory effect on organic anion transporting polypeptides*

In order to investigate whether OATP1B1 or OATP2B1 may interact with the amino acid conjugates and the reference HQ compounds, we analyzed their inhibitory potential on OATPs function, using a fluorescence–based cellular transport assay (Patik et al., 2018). Interaction with OATP1B1 was investigated at physiological pH (7.4), while the transport inhibition assay was performed at pH 5.5 in the case of OATP2B1, which is often upregulated in tumors and activated at acidic pH (Li et al., 2019; Schulte and Ho, 2019). The inhibitory effect of the compounds was monitored through the OATP-uptake of fluorescent disulfopyrene (OATP1B1) or pyranine (OATP2B1) test substrates in A431 epidermoid carcinoma cells engineered to overexpress OATPs. During the initial screen, the compounds were tested at 10 μM and 100 μM concentrations (Figure S14), then the effect of selected compounds (>50 % inhibition at 100 μM) were assayed in more detail to derive IC_{50} values (Table 6, Figure S15). Our earlier work has shown that $HQNO_2$-L-Pro has a minor inhibitory effect on OATP1B1 and OATP2B1. Interestingly, $HQNO_2$ proved to be a potent inhibitor of both OATPs, showing the strongest inhibitory effect on OATP2B1 (IC_{50} = 5.4 μM), while a lower inhibitory effect was observed on OATP1B1 (IC_{50} = 15.7 μM). HQCl-D-hPro shows modest inhibition on both transporters (28–36 μM), while the *L*/*D*-Pro-derivatives barely inhibit the two transporters. The lowest IC_{50} values obtained for $HQNO_2$, are comparable to data reported for taurocholate ($IC_{50(OATP1B1)}$ = 11.2 μM, $IC_{50(OATP2B1)}$ 12.3 μM), which is a weL-known substrate of both transporters, however they are much higher than those of estrone-3-sulfate ($IC_{50(OATP1B1)}$ = 0.22 μM, $IC_{50(OATP2B1)}$ = 0.56 μM) (Patik et al., 2018). It is important to note that this assay shows inhibition of transport of dye molecules, but it is not suitable to decide whether the present HQ derivatives are indeed substrates, like taurocholate and estrone-3-sulfate, or simple inhibitors of the transporters.

Considering the lipophilicity and charge of the compounds at the actual pH values (see data in Tables 3, 4 at pH 7.4 for OATP1B1 and pH 5.5 for OATP2B1) it is difficult to find a correlation with the OATP inhibitory effect. In the case of the reference compounds, the obtained data clearly show an increased inhibitory effect on the OATPs in the order of HQ < HQCl < $HQNO_2$, which follows the increased fraction of the anionic (L^-) forms at both pH values (Table 3). While in the case of the 5-chloro/nitro amino acid conjugates, no such correlation is found. Apparently, the D-enantiomers are stronger inhibitors than the L-derivatives. This finding again highlights the importance of the actual enantiomeric form (*D* or *L*) in interactions with biological macromolecules. It should be also noted that both $HQNO_2$ and $HQNO_2$-L-Pro are

Table 6
Effect of the HQ compounds on the transport activity of OATPs expressed as IC_{50} (μM) values, determined by nonlinear regression analysis of the data shown in Figure S15, using GraphPad prism software (GraphPad Prism, 2018).[a]

IC_{50} (μM)[b]	OATP1B1 (pH 7.4)	OATP2B1 (pH 5.5)
HQ	> 100	> 100
HQCl	57 ± 11	77.7 ± 5.9
$HQNO_2$	15.8 ± 4.3	5.3 ± 1.2
HQCl-L-Pro	> 100	> 100
HQCl-D-Pro	> 100	55.5 ± 9.1
HQCl-D-hPro	32.0 ± 6.1	29.5 ± 4.0
$HQNO_2$-L-Pro[c]	> 100	> 100

[a] Average (n = 3) ± SD values are shown.
[b] positive control sulfobromophthalein applied in 100 μM caused total inhibition of both transporters.
[c] data for $HQNO_2$-L-Pro are taken from Ref. (Pivarcsik et al., 2023).

found mostly in their −1 charged forms at pH 7.4, yet a big difference is seen between their effect on the transport activity. In general, OATP substrates are reported to be highly albumin bound in blood circulation (Schulte and Ho, 2019). This seems to be true for the present compounds, as $HQNO_2$, HQCl and HQCl-D-hPro, the three strongest binders of HSA, are able to exert appreciable inhibitory effect on OATP1B1 and OATP2B1, while the other derivatives, with lower albumin affinity, do not.

2.5. Molecular docking on the organic anion transporter binding of the molecules

Docking of the reference HQ compounds and their amino acid conjugates was carried out with a dual purpose. First, our aim was to locate binding sites for this set of compounds that could potentially be associated with the inhibition of transport activities of OATP1B1 and OATP2B1. Second, we wanted to compare putative binding modes of the *in vitro* effective inhibitors in order to deduce structural features responsible for their binding to the transporters. It should be noted, that comparison and assessment of inhibition constants obtained from docking studies and *in vitro* experiments is well founded only if the binding site of the studied compounds is known and also reproduced in dockings.

In the absence of high-resolution structures of OATP1B1 and OATP2B1. structural models of these proteins were used for the docking studies which were selected on the basis of completeness. Structures obtained from the AlphaFold Protein Structure Database were chosen over a previously published, validated structural model (Tuerkova et al., 2021) because, opposed to the latter, those included three out of four extended extracellular loops of both transport proteins on top of the N-terminal domains (NTDs) C-terminal domains (CTDs). Furthermore, the recently published cryoelectron microscopic (cryo-EM) structure of OATP1B1 (Shan et al., 2023) has confirmed the suitable accuracy of the AlphaFold-predicted structure (C_α RMSD = 1.087), which represents the inward-open state of the protein, observed when bound by estrone-3-sulfate. Numerous preferred binding locations were found in the first pass of docking, when the entire accessible surface of the proteins was scanned (Figure S16). The physical size, chemical composition and protonation state of the ligands varied notably and the docking targets were also set up in multiple protonation states. Consequently, searching for ligand-specific binding sites would have been elusive, hence it was omitted in this stage. Plausible binding sites were assigned when high frequency ligand localization was observed at a given site, with low binding free energies, and if binding to that site could sterically block the passage of endogenous substrates through the transmembrane domains of OATP1B1 and OATP2B1. Following this latter consideration, binding hot spots in the central cavity of the transmembrane domain and in the pore openings in either the intracellular or the extracellular surfaces were prioritized in the selection process over binding sites in the folds of the extracellular loops and on the intracellular tips of transmembrane helices. Furthermore, sites on the lipid interface of the transmembrane domain were not considered to be relevant. For OATP1B1, two adjacent sites in the central cavity of the transmembrane domain were selected for further refinement through flexible dockings. These two sites appear to be continuously joined, but closer analysis of the ligands bound in this region revealed that these are in fact separate sites, sharing only Phe^{356}. One of these binding sites is mainly located in the NTD, while other in the CTD, therefore they are referred to as N-terminal domain transmembrane binding site (NTD TM site) and C-terminal domain transmembrane binding site (CTD TM site) from this point on. For OATP2B1, a site analogous to that the NTD TM site of OATP1B1, and another in the cavity opening on the intracellular surface, further referred to as IC cavity opening site, were selected for further refinement (Figure S16).

Flexible docking of HQ compounds and their amino acid conjugates demonstrating OATP transport inhibition in the *in vitro* experiments to

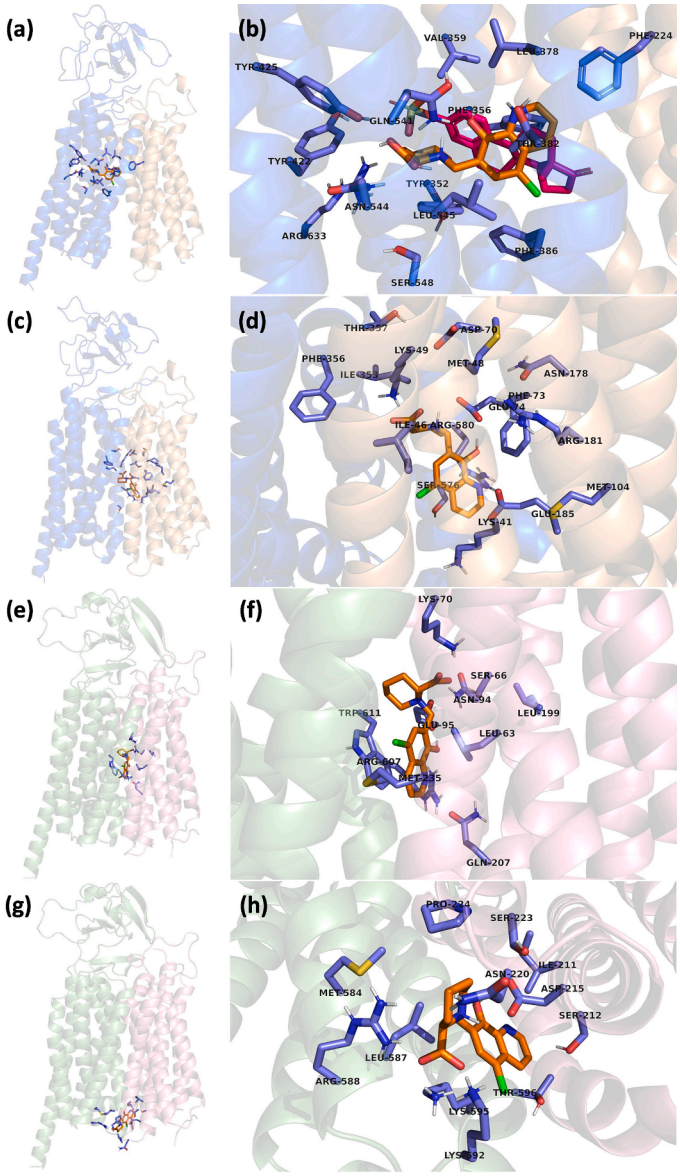

Fig. 10. Predicted binding sites of HQCl-D-hPro in OATP1B1 and OATP2B1. (a-b) CTD TM site in OATP1B1, experimentally derived coordinates of OATP1B1-bound estrone-3-sulfate are shown in magenta (PDB code: 8HND), (c-d) NTD TM site in OATP1B1 (e-f) NTD TM site in OATP2B1 (g-h) IC cavity opening site in OATP2B1. CTDs of OATP1B1 and OATP2B1 are colored in marine blue and pale green, respectively. NTDs of OATP1B1 and OATP2B1 are colored in wheat and light pink, respectively. Docked HQCl-D-hPro is shown in orange colored stick representation. Amino acid side chain lining the predicted pockets are shown in slate colored stick representation.

the above selected putative binding sites yielded refined binding poses, which allowed the identification of key amino acid residues that participate in the binding of this class of compounds. More accurate calculation of predicted inhibitory constants (Fig. 10, Table 7) was performed to assess and compare the predicted binding sites and the different ligands in light of their above reported *in vitro* inhibitory activity. The predicted transmembrane sites of OATP1B1 and OATP2B1 show good agreement with sites proposed previously on the basis of ensemble docking to comparative structural models of these proteins (Tuerkova et al., 2021). Moreover, the CTD TM site of OATP1B1 proposed here is in perfect agreement with the binding site of estrone-3-sulfate in OATP1B1, determined experimentally in a recent parallel study, as shown in Fig. 10b OATPs are generally characterized

Table 7
Predicted binding sites of OATP1B1 and OATP2B1 and ligand inhibitory constants.

Predicted binding site	Compound	Form	Δg/kcal mol^{-1}	Predicted k_i / nm*	Binding site residues
OATP1B1 CTD TM	HQCl	HL^0	−8.84	100–1000	Phe^{224}, Tyr^{352},
	HQCl $^-$	L	−8.41	100–1000	Phe^{356}, Val^{359},
	$HQNO_2$	HL^0	−11.44	1–10	Leu^{378}, Thr^{382},
	$HQNO_2$	L^-	−10.93	1–10	Phe^{386}, Tyr^{422},
	HQCl-D-hPro	H_2L^0	−10.07	10–100	Tyr^{425}, Gln^{541}, Asn^{544}, Leu^{545}, Ser^{548}, Arg^{633}
OATP1B1 NTD TM	HQCl	HL^0	−7.26	>1000	Lys^{41}, Met^{48},
	HQCl	L^-	−7.80	>1000	Lys^{49}, Phe^{73},
	$HQNO_2$	HL^0	−9.70	10–100	Glu^{74}, Met^{104},
	$HQNO_2$	L^-	−8.50	100–1000	Asn^{178}, Arg^{181},
	HQCl-D-hPro	H_2L^0	−10.05	10–100	Glu^{185}, Ile^{353}, Thr^{357}, Arg^{580}
OATP2B1 NTD TM	HQCl	HL^0	−8.57	100–1000	Leu^{63}, Ser^{66},
	$HQNO_2$	HL^0	−11.99	1–10	Lys^{70}, Asn^{94},
	$HQNO_2$	L^-	−11.97	1–10	Glu^{95}, Leu^{99},
	HQCl-D-hPro	H_2L^0	−13.15	0.1–1	Gln^{207}, Arg^{607}, Trp^{611}
	HQCl-D-hPro	HL^-	−11.80	1–10	
OATP2B1 IC cavity opening	HQCl	HL^0	−6.64	>10,000	Ile^{211}, Ser^{212},
	$HQNO_2$	HL^0	−10.59	10–100	Asp^{215}, Asn^{220},
	HQNO2	L^-	−9.77	10–100	Ser^{223}, Pro^{224},
	HQCl-D-hPro	H_2L^0	−10.69	10–100	Met^{584}, Leu^{587}, Arg^{588}, Lys^{592},
	HQCl-D-hPro	HL^-	−8.40	100–1000	Lys^{595}, Thr^{596}

* Range / order of magnitude of the predicted inhibitory constants of the lowest binding free energy docked poses of each compound.

by very broad substrate specificity, which suggest that compounds with significantly different chemical structures, such as steroids and the compounds addressed in this study can be accommodated in the same binding site. Predicted inhibitory constants of HQ compounds and their conjugates indicate a slight preference for the CTD TM site in OATP1B1. Nevertheless, the NTD TM site and the analogous site in OATP2B1 could also be deemed relevant, as most of the amino acid residues of those sites were indicated to be important for transport activity in previous reports (Tuerkova et al., 2021 Shan et al., 2023; Li et al., 2012; Hong et al., 2015). The highest affinity for the CTD TM site of OATP1B1 was indicated for $HQNO_2$, regardless of its protonation state (Tables 3, 4). Moreover, inhibitory constants calculated for HQCl, $HQNO_2$ and HQCl-D-hPro are in good agreement with the trend observed in the *in vitro* transport inhibition experiments (Table 6), suggesting that stronger association between these compounds and the transport protein leads to higher inhibitory effects. The IC cavity entrance site, found here for OATP2B1, have not received much attention previously. Relatively strong association of the studied compounds and the IC cavity entrance site of OATP2B1 could be exploited in the design of novel transport inhibitors. Penetration of ligands into this cavity entrance (Fig. 10 g–h) could block 'rocker-switch' motions, a recently proposed structural mechanism of action of this protein class (Shan et al., 2023).

3. Conclusions

There is a growing need for the development of targeted, effective treatments for drug-resistant cancers. Overexpression of P-glycoprotein, a cell membrane efflux pump, is one of the main causes of resistance. Interestingly, the presence of this drug efflux pump in cell membrane can also make MDR cancer cells vulnerable through a mechanism that leads to the depletion of essential metal ions, ultimately resulting in cell death. This mechanism has been previously demonstrated for structurally close analogs of the present 8-hydroxyquinoline Mannich base compounds. HQCl-L-Pro, HQCl-D-Pro, HQCl-D-hPro $HQNO_2$-L-Pro, 5-chloro-7-(pyrrolidin-1-ylmethyl)quinolin-8-ol, 5-chloro-7-(piperidin-1-ylmethyl)quinolin-8-ol and 7-(1-piperidinylmethyl)-8-hydroxyquinoline showed also enhanced toxicity on MDR cancer cells (Pivarcsik et al., 2023; Pivarcsik et al., 2024; Dömötör et al., 2017; Mészáros et al., 2020; Pivarcsik et al., 2021). In the present study we have investigated the zwitterionic proline and homoproline derivatives. We aimed to explore how the different structural and physicochemical properties affect cytotoxicity and MDR selectivity, and whether there is any trend in the HSA binding and OATP inhibition of the molecules. To this end, we provided a comprehensive analysis of the cytotoxicity of these compounds on both parental and Pgp-expressing MDR cancer cells, characterized their solution chemical properties, evaluated their binding to human serum albumin, and assessed their inhibitory effects on OATP1B1 and OATP2B1 transporters.

We have developed molecules that are water-soluble, yet their lipohydrophilic character is favorable. The reference molecules HQ, HQCl and $HQNO_2$ were cytotoxic with IC_{50} values in the low micromolar range; and showed similar anticancer activity against parental and MDR cells. In contrast, the selected HQCl–Mannich bases are moderately cytotoxic against parental MES-SA cells but exhibited increased antitumor activity on Pgp-expressing MDR MES-SA/Dx5 cells. Albumin is a likely carrier of the 5R-chloro and 5R-nitro derivatives in human blood, thus contributing to targeted drug delivery. At least two binding sites are available in HSA for the studied molecules. The strongest overall binding was found for $HQNO_2$, HQCl-D-hPro and HQCl. The binding affinities and orientation of the two enantiomers of HQCl-Pro in the binding sites are different in favor of the D-enantiomer, indicating the importance of exploring the interactions of different enantiomeric forms (*D* or *L*) with biological macromolecules. *In vitro* OATP inhibition assays indicated that $HQNO_2$, HQCl and HQCl-D-hPro are able to exert appreciable inhibitory effect on OATP1B1 and OATP2B1, however, based on this assay it cannot be decided whether the molecules are also substrates of these membrane transporters. Based on docking studies the CTD TM site in OATP1B1 is the preferred site of the studied HQ compounds. The NTD TM sites in both transporters are also considered relevant in binding of these HQ derivatives. The highest affinity for the CTD TM site of OATP1B1 was indicated for $HQNO_2$, regardless of its protonation state. Relatively strong association of the studied compounds and the IC cavity entrance site of OATP2B1 could be exploited in the design of novel transport inhibitors.

The following correlations were found between the anticancer activity, the cell membrane or blood transport protein binding and the physico-chemical properties. For parental MES-SA cells a broadly linear relationship was found between the negative decadic logarithm of the IC_{50} (pIC_{50}) values and log*D* at pH 7.4. The $logD_{7.4}$ values also show some weak correlations with HSA binding. And finally, only strong albumin binder molecules $HQNO_2$, HQCl and HQCl-D-hPro are able to exert appreciable inhibitory effect on OATP1B1 and OATP2B1. These results certainly enrich our knowledge of MDR HQs and tailor the direction for further research.

4. Materials and methods

4.1. Chemicals

The solvents used, dimethyl sulfoxide, *n*-octanol, were of analytical grade and used without further purification. KCl, NaCl, KI, KOH, NaH_2PO_4, Na_2HPO_4, KH_2PO_4, disodium-EDTA, HCl solution are product of VWR, Molar Chemicals, or Reanal. D_2O, HQ, HQCl, $HQNO_2$, DG, WF, BR, doxorubicin, 6,8-disulfopyrene (6,8-dihydroxy-1,3-pyrenedisulfonic acid disodium salt), pyranine (8-hydroxypyrene-1,3,6-trisulfonic acid trisodium salt), sulfobromophthalein, HSA (A8763, essentially globulin free), human blood serum (H4522, male AB plasma) were purchased from Sigma Aldrich. HQCl-L-Pro, HQCl-D-Pro, HQCl-D-hPro and $HQNO_2$-L-Pro were synthesized as reported formerly (Mészáros et al., 2020; Pivarcsik et al., 2021; Pivarcsik et al., 2023).

4.2. Stock solutions and sample preparation

Doubly distilled Milli-Q water was used for sample preparation. Samples for albumin binding studies were prepared in modified phosphate-buffered saline (PBS') or in PBS' containing 2 mM Na_2EDTA at pH = 7.4. PBS' contains 12 mM Na_2HPO_4, 3 mM KH_2PO_4, 1.5 mM KCl, and 100.5 mM NaCl; the concentrations of K^+, Na^+, and Cl^- ions corresponds to the human blood serum levels. Protein stock solutions were prepared in PBS' buffer and their concentration was calculated on the basis of their UV–vis absorption: $\varepsilon_{280\ nm}$(HSA) = 36,850 M^{-1} cm^{-1} (Beaven et al., 1974). Stock solutions of HQ, HQCl and $HQNO_2$ were prepared as basic aqueous solutions (1–5 mM, pH = 10–11), the other compounds HQCl-*L/D*-Pro, HQCl-D-hPro and $HQNO_2$-L-Pro could be dissolved in pure water (1–3 mM). The concentrations were determined by pH-potentiometric titrations and on weight-in-volume basis for the synthesized and the marketed compounds, respectively (Enyedy et al., 2012). In HSA binding experiments these stocks were diluted with water to get the working solutions (c = 50–400 μM). Human serum was diluted with PBS' buffer.

4.3. Cytotoxicity assay

All cell culture reagents were obtained from Merck llc. (Budapest, Hungary); plastic ware was purchased from VWR International llc. (Budapest, Hungary); MES-SA and MES-SA/Dx5 uterine sarcoma cell lines were obtained from ATCC, where they were characterized by DNA fingerprinting. The MES-SA/B1 cell line was created by the insertion of the MDR1 gene, and MES-SA, MES-SA/Dx5 and MES-SA/B1 cells used in this study were previously engineered to express the fluorescent proteins mCherry eGFP and mOrange, respectively, by lentiviral transduction (Windt et al., 2019). MES-SA cell lines were maintained in DMEM, supplemented with 10 % fetal bovine serum, 5 mM glutamine, and 50 units/mL penicillin and streptomycin. Cells were tested and resulted negative for mycoplasma contamination with the MycoAlert mycoplasma detection Kit (Lonza Group, Basel, Switzerland). One week prior to the cytotoxicity assays, Dx5 eGFP and B1 mOrange cells were selected in 500 nM doxorubicin for one passage to ensure the overexpression of Pgp. The tested compounds were dissolved in DMSO to prepare 10 mM stock solutions, which were diluted in complete culture medium. Cells were seeded at a final cell density of 2400 cells per well in 384-well plates in the triple coculture (800 cells from each lines). After an overnight incubation, a serial dilution of the compounds was added to the plate in a final volume of 60 μL. The Pgp inhibitor tariquidar was added to the cells 15 min prior to the test compounds. After 144 h of incubation, plates were measured for the fluorescent intensity of mCherry (EX/EM: 585 nm/610 nm), eGFP (EX/EM: 485 nm/510 nm) mOrange (EX/EM: 545 nm/567 nm). Cell seeding, aspiration of medium, and addition of drugs were performed by a Hamilton StarLet automated liquid handling robot. Data were exported to a custom-made program (written by J. Sessler in C#) for determining growth inhibition curves and then IC_{50} values for each cell line. As the cell lines interact with each other in the coculture system (the surviving cell line has growth advantage, which translates into viability values exceeding 100 %), curve fitting was not suitable. Therefore, pIC_{50} values were identified as the intersection of the line of connected viability values and the 50 % viability, and the respective logarithm of the concentration was calculated (for visualization, see Figure S1). The *p* values were calculated by Student's *t*-test. The IC_{50} values were always obtained from at least three independent experiments.

4.4. UV–vis spectrophotometric measurements

An Agilent Cary 8454 diode array spectrophotometer was used to obtain UV–vis spectra in the interval 190–1100 nm, the path length (ℓ) was 1 or 2 cm. UV–vis detection was used (i) to determine proton dissociation processes of HQCl and $HQNO_2$ and (ii) lipophilicity at various pH values, (iii) to study the HSA binding directly, (iv) to analyze ultrafiltered phases and (v) to correct spectrofluorometric data by absorption. pH-dependent spectrophotometric titrations were performed with samples containing 20–60 μM compound (HQCl, $HQNO_2$) over the pH range 2.0–11.5 at 25.0 ± 0.1 °C and an ionic strength of 0.10 M (KCl). Calibration of the system and titrations were done according to literature procedures (Dömötör et al., 2024; Irving et al., 1967). Proton dissociation constants together with the individual molar absorbance spectra were calculated with the computer program HypSpec (Gans et al., 1996).

For the albumin binding assays the HQ derivatives' concentration was kept constant (20–110 μM depending on the solubility and molar absorptivity of the compound) and the HSA concentration was varied between 0 and 150 μM. UV–vis spectra shown in this work are subtracted by the absorbance of HSA.

4.5. Lipophilicity

Distribution coefficients (D_{pH}) of the compounds were determined by the traditional shake-flask method in *n*-octanol/buffered aqueous solution generally at pH 2.1 (HCl), pH 5.5 (MES) and pH 7.4 (PBS') at 25.0 ± 0.2 °C as described previously (Enyedy et al., 2011). The compounds were dissolved in *n*-octanol pre-saturated aqueous solution of the buffer (50–100 μM Then the aqueous sample was mixed with *n*-octanol in 1:1, 10:1 or 1:10 vol ratio in a vertical rotating shaker (3 h, *ca.* 30 rpm). Afterwards, the two phases were separated in an Eppendorf MiniSpin plus centrifuge (5 min, 10^4 rpm). At least two parallel measurements were done. HQCl alternatively was dissolved in *n*-octanol presaturated with water (*ca.* 200 μM) then it was mixed with the aqueous buffer in 1:10 vol ratio and treated according to the usual protocol. After phase separation, UV–vis spectrum of the compound in the aqueous phase was compared to that of the original stock solution and D_{pH} value of the compounds was calculated according to the formula $D_{pH} = [(Abs_{(aqueous\ stock\ solution)} / Abs_{(aqueous\ phase\ after\ separation)}) - 1] \times (V_{aqueous\ phase} / V_{n\text{-}octanol})$. For HQCl the applied formula is: $D_{pH} = [Abs_{(n\text{-}octanol\ after\ separation)} / (Abs_{(n\text{-}octanol\ stock\ solution)} - Abs_{(n\text{-}octanol\ after\ separation)})] \times (V_{aqueous\ phase} / V_{n\text{-}octanol})$.

4.6. Ultrafiltration

Samples were separated by ultrafiltration through 10 kDa membrane filters (Millipore, Amicon Ultra-0.5) into low and high molecular mass (LMM and HMM) fractions as described in our former work (Dömötör and Enyedy, 2019). Samples contained 50 or 100 μM HQ-compound and 0.5 equivalent HSA. In the case of $HQNO_2$ samples contained 40 μM ligand and 0–120 μM HSA. The concentration of the non-bound compounds in the LMM fractions was determined by UV–vis spectrophotometry by comparing the recorded spectra to those of reference samples without the protein. Blood serum was diluted to 12.6-fold or 25-fold considering the average HSA concentration (630 μM) of blood serum to obtain similar compositions comparable with those measurements with only HSA (50 or 25 μM). The recorded UV–vis spectra were corrected with the spectrum of the ultrafiltrated blood serum, since it possesses significant absorbance between 200 and 300 nm. The compound's adhesion to the filter was taken into account in our calculations, the filtration efficacy for each compound is listed in Table S3.

4.7. Circular dichroism spectroscopy

CD spectroscopic experiments were performed by a JASCO-J-1500 spectrometer. Samples contained (i) 2 μM HSA and 0–80 μM HQ-compound using 2 mm path length or (ii) 43 or 100 μM *L/D*-(h)Pro derivative and 0–150 μM HSA using 1 cm path length.

4.8. Saturation transfer difference NMR spectroscopy

The ^{1}H STD NMR spectra were recorded on a Bruker AVANCE III 600 MHz spectrometer equipped with a 5 mm CP-TCI triple-resonance cryoprobe at 280 K. The compounds were dissolved in phosphate buffer (20 mM, pH 7.4) containing 10 % (v/v) D_2O. ^{1}H STD spectra were acquired with water suppression using excitation sculpting with pulsed gradients. For the STD measurements, the concentration of the ligands were 50 or 100 μM and the HSA concentration was 10 μM. The samples were placed in 5 mm NMR tubes. As a reference, STD experiments were also performed without the target in samples that contained the ligand species alone. STD NMR spectra were acquired using a series of 40 equally spaced 50 ms Gaussian-shaped pulses for selective saturation of the protein, with a total saturation time of 2 s. The frequency of the *on*-resonance saturation was set at 0.6 ppm, and the *off*-resonance saturation frequency was set at 40.0 ppm. A total of 512 scans were collected for each pseudo-2D experiment. STD amplification was calculated according to the formula $STD_{amp} = [(\int_0 - \int_{sat}) / \int_0] \times (c_{lig} / c_{HSA})$, where $\int_0$ and $\int_{sat}$ are the peak integrals of the ligand recorded at *off*-resonance and *on*-resonance frequencies, respectively; c_{lig} and c_{HSA} are the analytical concentrations of the small molecule and HSA (Viegas et al., 2011; Mayer and Meyer, 2001). Relative STD_{amp} values are normalized to the highest STD_{amp} of the molecule and expressed in %.

4.9. Fluorescence spectroscopy

Fluorescence studies were implemented by a Fluoromax (Horiba Jobin Yvon) fluorometer in 1 × 1 cm quartz cells. Sample composition and instrument settings for the Trp^{214} quenching, and site marker displacement (WF, DG, BR) experiments are listed in Table S4. The computer program HypSpec (Gans et al., 1996) was utilized for calculation of binding constants (*K*') for HSA–compound adducts similar to the approach described in our former works (Dömötör et al., 2013; Enyedy et al., 2015). Whole emission spectra were used for calculations. WF and DG were also applied as binding standards at the respective sites, the binding constants obtained (log*K*' = 5.6 (HSA-WF) and 5.3 (HSA-DG)) are in good agreement with our previous results (Dömötör et al., 2013). Calculations were always based on data obtained from at least two independent measurements. Measured intensities were corrected for self-absorbance and inner filter effect according to our former works using the formula suggested by Lakowicz (Lakowicz, 2006; Dömötör et al., 2013; Dömötör and Enyedy, 2019).

Fluorescence lifetimes were measured using the same fluorometer equipped with a DeltaHub time correlated single photon counting controller using NanoLED light sources N-295 (Horiba Jobin Yvon). See details on the instrument settings in Table S5. Ludox® (from Sigma-Aldrich) was used as a scatter solution to obtain the instrument response function. The background (obtained with the blank sample) was subtracted from the decay. The program DAS6 (version 6.6.; Horiba Jobin Yvon) was used for the analysis of the experimental fluorescence decays. The fluorescence intensity decay over time is described by a sum of exponentials in eq. (1),

$$I(t) = \sum_{i=1}^{n} I_{0i} exp\left(\frac{-t}{\tau_i}\right) \quad (1)$$

where I_{0i} and τ_i are the contribution to the total intensity (I) at time point 0 and lifetime of component *i*, respectively. Better known is the formula that contains the normalized amplitude values α_i ($\sum\alpha_i = 1$) instead of I_{0i} (Lakowicz, 2006). From these parameters, the fraction of emitted light (f) by each component *i* can be calculated using Eq. (2).

$$f_i = \frac{\alpha_i \tau_i}{\sum(\alpha_i \tau_i)} \quad (2)$$

The quality of the fit was judged from a χ^2_R value ($\chi^2_R \leq 1.20$) and a random distribution of weighted residuals. The construction of decay associated spectra for the HSA–WF–$HQNO_2$ system was made according to our former work, detailed description and instrument settings are found in the Supplementary Materials (Table S5 and Section S4) (Dömötör et al., 2021).

4.10. Organic anion transporting protein uptake assays

A431 cells overexpressing OATP1B1 or OATP2B1, and their mock transfected controls were generated and characterized previously (Patik et al., 2018). The assays were conducted as reported in our former work (Pivarcsik et al., 2023). Briefly, the cell lines were cultured in DMEM (Gibco, Thermo Fisher Scientific, Waltham, MA, USA), supplemented with 10 % fetal bovine serum, 2 mM L-glutamine, 100 μg/mL streptomycin, and 100 units/mL penicillin at 37 °C and 5 % CO_2. Prior to the experiment, A431 cells were seeded on 96-well plates (8×10^4/well) in 200 μL cell culture medium. After 16–24 h, the cells were washed with 200 μL PBS, three times and pre-incubated with 10 or 100 μM (initial screen) or 0.16–100 μM HQ-compound, or buffer without compound 5 min at 37 °C in 50 μL HBSS (Hank's Balanced Salt Solution, pH 7.4; OATP1B1) or uptake buffer (pH 5.5; OATP2B1 (Patik et al., 2018)). The reaction was started by the addition of disulfopyrene at a final concentration of 10 μM (OATP1B1) or pyranine at a final concentration of 20 μM (OATP2B1), and the cells were further incubated at 37 °C for 10 min (OATP1B1) or 15 min (OATP2B1). The reaction was stopped by removing the supernatant after which the cells were washed three times with ice-cold PBS. Fluorescence (in 200 μL PBS) was determined using an Enspire plate reader (PerkinElmer, Waltham, MA, USA) with excitation/emission wavelengths of 460/510 nm. Sulfobromophthalein (100 μM) was used as positive control, which resulted in complete inhibition of OATP1B1 and OATP2B1. OATP-dependent transport was calculated by subtracting fluorescence measured in mock transfected cells. Transport activity was calculated based on the fluorescence signal in the absence (100 %) of flavonoids. Experiments were repeated in at least three replicates.

4.11. Molecular docking

Structural models of human OATP1B1 and OATP2B1 (Uniprot IDs: Q9Y6L6 and O94956, respectively) were obtained from the AlphaFold Protein Structure Database (AlphaFold, 2022; Jumper et al., 2021). Low confidence structural regions of the models with pLDDT scores lower that 70 have been truncated. The structures of OATP1B1 and OATP2B1 used as targets for docking included the N- and C-terminal transmembrane domains (NTD and CTD, respectively) and extended extracellular loops connecting the 5th and 6th (EL5–6), 9th and 10th (EL9–10, Kazal domain) and 11th and 12th transmembrane helices (EL11–12). Protonation states of the constituent amino acids of both transporter proteins, corresponding to pH 5.5 and pH 7.4 were set using the PropKa server (PropKa, 2004–2021, Li et al., 2005) Coordinate files of HQ ligands and their amino acid conjugates were built using the Pymol 2.4.0 software (Schrödinger LLC, New York, NY, USA) including all possible protonation states at pH 5.5 and pH 7.4 (Tables 3–4). To scan the accessible surface of the target proteins for potential binding sites, blind dockings were performed using the Autodock 4.2 software and the Lamarckian genetic algorithm with default parameters. The maximum of energy evaluations was set to 2500,000 and the spacing of grid points was set to 0.375 Å. Parallel dockings as a representation of free, unbiased ligand association with the target protein were performed in two overlapping 46.875 Å × 46.875 Å × 46.875 Å volume grids, which together were large enough to cover the whole surface of the transmembrane domain accessible form either the extracellular or the intracellular side. Protein structures were kept rigid during dockings, while ligand structures were treated fully flexible. 1000 dockings were performed with the above settings for each ligand and target protein in their respective protonation states, corresponding to either pH 5.5 or pH 7.4, resulting in 116 parallel docking calculations. The obtained

ligand-OATP complexes were grouped on the basis of structural similarity by clustering with 2.0 Å tolerance and ranked according to their calculated binding free energies. The 10 best scoring cluster representatives of each docking setup were included in further analysis and putative binding sites were assigned on the basis of ligand localization frequency. The selected, most populated binding poses were subjected to further refinement by a second pass of docking, where amino acid side chains of OATPs, identified in the previous pass to be in close contact with the ligands (< 4.0 Å), were kept flexible. Grid volumes were reduced to these putative binding sites including all flexible amino acid side chains (27.75 Å × 27.75 Å × 27.75 Å), where the spacing of grid points was maintained at 0.375 Å. Only those ligands were included in the second pass, which exerted considerable effect on the transport activities of OATP1B1 and OATP2B1 in the respective *in vitro* disulfopyrene and pyranine uptake experiments. Furthermore, in the second pass, OATP1B1 and OATP2B1 were only investigated at pH 7.4 and pH 5.5, respectively, in accordance with the conditions of the aforementioned experiments. Putative binding sites and binding modes of the studied ligands were proposed on the basis of binding free energies and the number of direct intermolecular contacts. *In silico* inhibitory constants were calculated from binding free energies derived from docking, according to the following equation: $\Delta G = RT \ln K_i$.

CRediT authorship contribution statement

Orsolya Dömötör: Writing – review & editing, Writing – original draft, Investigation. **Tamás Pivarcsik:** Investigation. **Zeinab Nezafat Yazdi:** Investigation. **Éva Bakos:** Investigation. **Csilla Özvegy-Laczka:** Resources, Funding acquisition. **Anasztázia Hetényi:** Investigation. **Tamás Martinek:** Resources. **István Szatmári:** Investigation. **Szilárd Tóth:** Investigation. **Gergely Szakács:** Writing – review & editing, Resources. **Attila Borics:** Writing – review & editing, Writing – original draft, Investigation. **Éva A. Enyedy:** Writing – review & editing, Resources, Funding acquisition, Conceptualization.

Declaration of competing interest

The authors declare no conflict of interest.

Acknowledgments

The work was supported by the National Research, Development and Innovation Fund through projects ANN 149481(É.A.E.), K 138518 (C.Ö.-L.), and K 143124 (A.B.). Project no TKP2021-EGA-32 was implemented with the support provided by the Ministry of Culture and Innovation of Hungary from the National Research, Development and Innovation Fund, financed under the TKP2021-EGA funding scheme. Austrian Science Fund supported this research through project FWF 10.55776/PIN1280424 (S.G.).

Declaration of generative AI in scientific writing

The authors state that AI-assisted technology was only used in the writing process to improve the readability and language of the manuscript.

Supplementary materials

Supplementary material associated with this article can be found, in the online version, at doi:10.1016/j.ejps.2025.107187.

Data availability

Data will be made available on request.

References

AlphaFold, 2022. AlphaFold Protein Structure Database. https://alphafold.ebi.ac.uk/ (Accessed 3 March 2025).

Beaven, G.H., Chen, S., D'Albis, A., Gratzer, W.B., 1974. A spectroscopic study of the haemin-human-serum-albumin system. Eur. J. Biochem. 42, 539–546. https://doi.org/10.1111/j.1432-1033.1974.tb03295.x.

Bristol-Myers Squibb Canada, 2018. Product monograph of Coumadin. https://pdf.hres.ca/dpd_pm/00047189.PDF.

Chadborn, N., Bryant, J., Bain, A.J., O'Shea, P., 1999. Ligand-dependent conformational equilibria of serum albumin revealed by tryptophan fluorescence quenching. Biophys. J. 76, 2198–2207. https://doi.org/10.1016/S0006-3495(99)77375-3.

Cserepes, M., Türk, D., Tóth, S., Pape, V.F.S., Gaál, A., Gera, M., Szabó, J.E., Kucsma, N., Várady, G., Vértessy, B.G., Streli, C., Szabó, P.T., Tovari, J., Szoboszlai, N., Szakács, G., 2020. Unshielding multidrug resistant cancer through selective iron depletion of P-glycoprotein–expressing cells. Cancer Res. 80, 663–674. https://doi.org/10.1158/0008-5472.can-19-1407.

DeSimone, R.W., Currie, K.S., Mitchell, S.A., Darrow, J.W., Pippin, D.A., 2004. Privileged structures: applications in drug discovery. Comb. Chem. High. Throughput Screen 7, 473–494. https://doi.org/10.2174/1386207043328544.

Dömötör, O., Hartinger, C.G., Bytzek, A.K., Kiss, T., Keppler, B.K., Enyedy, É.A., 2013. Characterization of the binding sites of the anticancer ruthenium(III) complexes KP1019 and KP1339 on human serum albumin via competition studies. J. Biol. Inorg. Chem. 18, 9–17. https://doi.org/10.1007/s00775-012-0944-6.

Dömötör, O., Pape, V.F.S., May, N.V., Szakács, G., Enyedy, É.A., 2017. Comparative solution equilibrium studies of antitumor ruthenium(η6-p-cymene) and rhodium(η5-C5Me5) complexes of 8-hydroxyquinolines. Dalton Trans. 46, 4382–4396. https://doi.org/10.1039/C7DT00439G.

Dömötör, O., Enyedy, É.A., 2019. Binding mechanisms of half-sandwich Rh(III) and Ru(II) arene complexes on human serum albumin: a comparative study. J. Biol. Inorg. Chem. 24, 703–719. https://doi.org/10.1007/s00775-019-01683-0.

Dömötör, O., Pivarcsik, T., Mészáros, J.P., Szatmári, I., Fülöp, F., Enyedy, É.A., 2021. Critical factors affecting the albumin binding of half-sandwich Ru(II) and Rh(III) complexes of 8-hydroxyquinolines and oligopyridines. Dalton Trans. 50, 11918–11930. https://doi.org/10.1039/D1DT01700D.

Dömötör, O., Keppler, B.K., Enyedy, É.A., 2022. Solution speciation and human serum protein binding of indium(III) complexes of 8-hydroxyquinoline, deferiprone and maltol. J. Biol. Inorg. Chem. 27, 315–328. https://doi.org/10.1007/s00775-022-01935-6.

Dömötör, O., Mathuber, M., Kowol, C.R., 2024. *In vitro* biodistribution studies on clinically approved FGFR inhibitors ponatinib, nintedanib, erlotinib and the investigational inhibitor KP2692. Eur. J. Pharm. Sci. 192, 106651. https://doi.org/10.1016/j.ejps.2023.106651.

Dong, J., Yuan, L., Hu, C., Cheng, X., Qin, J.J., 2023. Strategies to overcome cancer multidrug resistance (MDR) through targeting P-glycoprotein (ABCB1): an updated review. Pharmacol. Ther. 249, 108488. https://doi.org/10.1016/j.pharmthera.2023.108488.

Duarte, C.D., Barreiro, E.J., Fraga, C.A., 2007. Privileged structures: a useful concept for the rational design of new lead drug candidates. Mini. Rev. Med. Chem. 7, 1108–1119. https://doi.org/10.2174/138955707782331722.

Elsadek, B., Felix Kratz, F., 2012. Impact of albumin on drug delivery — New applications on the horizon. J. Control Release 157, 4–28. https://doi.org/10.1016/j.jconrel.2011.09.069.

Enyedy, É.A., Hollender, D., Kiss, T., 2011. Lipophilicity of kinetically labile metal complexes through the example of antidiabetic Zn(II) and VO(IV) compounds. J. Pharm. Biomed. Anal. 54, 1073–1081. https://doi.org/10.1016/j.jpba.2010.12.025.

Enyedy, É.A., Dömötör, O., Varga, E., Kiss, T., Trondl, R., Hartinger, C.G., Keppler, B.K., 2012. Comparative solution equilibrium studies of anticancer gallium(III) complexes of 8-hydroxyquinoline and hydroxy(thio)pyrone ligands. J. Inorg. Biochem. 117, 189–197. https://doi.org/10.1016/j.jinorgbio.2012.08.005.

Enyedy, É.A., Dömötör, O., Bali, K., Hetényi, A., Tuccinardi, T., Keppler, B.K., 2015. Interaction of the anticancer gallium(III) complexes of 8-hydroxyquinoline and maltol with human serum proteins. J. Biol. Inorg. Chem. 20, 77–88. https://doi.org/10.1007/s00775-014-1211-9.

Füredi, A., Tóth, S., Szebényi, K., Pape, V.F.S., Türk, D., Kucsma, N., Cervenak, L., Tóvári, J., Szakács, G., 2017. Identification and validation of compounds selectively killing resistant cancer: delineating cell line–Specific effects from P-glycoprotein–Induced toxicity. Mol. Cancer Ther. 16, 45–56. https://doi.org/10.1158/1535-7163.mct-16-0333-t.

Gans, P., Sabatini, A., Vacca, A., 1996. Investigation of equilibria in solution. Determination of equilibrium constants with the HYPERQUAD suite of programs. Talanta 43, 1739–1753. https://doi.org/10.1016/0039-9140(96)01958-3.

GraphPad Prism, 2018. GraphPad Software, version 7.00 for Windows, La Jolla, California, USA. http://www.graphpad.com (Accessed 3 March 2025).

Hong, W., Wu, Z., Fang, Z., Huang, J., Huang, H., Hong, M., 2015. Amino acid residues in the putative transmembrane domain 11 of Human organic anion transporting polypeptide 1B1 dictate transporter substrate binding, stability, and trafficking. Mol. Pharmaceutics 12, 4270–4276. https://doi.org/10.1021/acs.molpharmaceut.5b00466.

Irving, H.M., Miles, M.G., Pettit, L.D., 1967. A study of some problems in determining the stoicheiometric proton dissociation constants of complexes by potentiometric titrations using a glass electrode. Anal. Chim. Acta 38, 475–488. https://doi.org/10.1016/S0003-2670(01)80616-4.

Jumper, J., Evans, R., Pritzel, A., et al., 2021. Highly accurate protein structure prediction with AlphaFold. Nature 596, 583–589. https://doi.org/10.1038/s41586-021-03819-2.

Karlsson, B.C.G., Rosengren, A.M., Andersson, P.O., Nicholls, I.A., 2007. The spectrophysics of warfarin: implications for protein binding. J. Phys. Chem. B 111, 10520–10528. https://doi.org/10.1021/jp072505i.

Klofutar, C., Paljk, Š., Krašovec, F., 1975. Thermodynamics of deprotonation and dissociation steps of 8-hydroxyquinoline, 5-chloro-8-hydroxyquinoline and 5-nitro-8-hydroxyquinoline in aqueous media. Spectrochim. Acta A 31, 1093–1097. https://doi.org/10.1016/0584-8539(75)80089-4.

Kounnis, V., Ioachim, E., Svoboda, M., Tzakos, A., Sainis, I., Thalhammer, T., Steiner, G., Briasoulis, E., 2011. Expression of organic anion-transporting polypeptides 1B3, 1B1, and 1A2 in human pancreatic cancer reveals a new class of potential therapeutic targets. Onco Targets. Ther. 4, 27–32. https://doi.org/10.2147/ott.s16706.

Lakowicz, J.R., 2006. Principles of Fluorescence Spectroscopy, 3rd ed. Springer, New York.

Li, H., Robertson, A.D., Jensen, J.H., 2005. Very fast empirical prediction and interpretation of protein pKa values. Proteins. 61, 704–721. https://doi.org/10.1002/prot.20660.

Li, N., Hong, W., Huang, H., Lu, H., Lin, G., Hong, M., 2012. Identification of amino acids essential for estrone-3-sulfate transport within transmembrane domain 2 of organic anion transporting polypeptide 1B1. PLoS ONE 7, e36647. https://doi.org/10.1371/journal.pone.0036647.

Li, T.T., An, J.-X., Xu, J.-Y., Tuo, B.-G., 2019. Overview of organic anion transporters and organic anion transporter polypeptides and their roles in the liver. World J. Clin. Cases 7, 3915–3933. https://doi.org/10.12998/wjcc.v7.i23.3915.

Lytle, F.E., Storney, D.R., Juricich, M.E., 1973. Systematic atomic number effects in complexes exhibiting ligand luminescence. Spectrochim. Acta. 298, 1357–1369. https://doi.org/10.1016/0584-8539(73)80199-0.

Mayer, M., Meyer, B., 2001. Group epitope mapping by saturation transfer difference NMR to identify segments of a ligand in direct contact with a protein receptor. J. Am. Chem. Soc. 123, 6108–6117. https://doi.org/10.1021/ja0100120.

Mészáros, J.P., Poljarevic,´ J.M., Szatmári, I., Csuvik, O., Fülöp, F., Szoboszlai, N., Spengler, G., Enyedy, É.A., 2020. An 8-hydroxyquinoline−proline hybrid with multidrug resistance reversal activity and the solution chemistry of its half-sandwich organometallic Ru and Rh complexes. Dalton Trans. 49, 7977–7992. https://doi.org/10.1039/D0DT01256D.

Müller, F., Fromm, M.F., 2011. Transporter-mediated drug-drug interactions. Pharmacogenomics 12, 1017–1037. https://doi.org/10.2217/pgs.11.44.

Nicholls, I.A., Karlsson, B.C.G., Rosengren, A.M., Henschel, H., 2010. Warfarin: an environment-dependent switchable molecular probe. J. Mol. Recognit. 23, 604–608. https://doi.org/10.1002/jmr.1058.

Nozawa, T., Imai, K., Nezu, J.I., Tsuji, A., Tamai, I., 2004. Functional characterization of pH-sensitive organic anion transporting polypeptide OATP-B in human. J. Pharmacol. Exp. Ther. 308, 438–445. https://doi.org/10.1124/jpet.103.060194.

Paljk, Š., Klofutar, C., Krašovec, F., Suhac, M., 1975. Dissociation of 8-hydroxyquinoline and its 5-chloro- and 5-nitro-derivatives in aqueous solutions. Mikrochim. Acta 64, 485–492.

Pape, V.F.S., May, N.V., Gál, G.T., Szatmári, I., Szeri, F., Fülöp, F., Szakács, G., Enyedy, É. A., 2018. Impact of copper and iron binding properties on the anticancer activity of 8-hydroxyquinoline derived Mannich bases. Dalton Trans. 47, 17032–17045. https://doi.org/10.1039/C8DT03088J.

Pape, V.F.S., Gaál, A., Szatmári, I., Kucsma, N., Szoboszlai, N., Streli, C., Fülöp, F., Enyedy, É.A., Szakács, G., 2021. Relation of metal binding property and selective toxicity of 8-hydroxyquinoline derived Mannich bases targeting multidrug resistant cancer cells. Cancers 13, 154. https://doi.org/10.3390/cancers13010154.

Pape, V.F.S., Palkó, R., Tóth, S., Szabó, M.J., Sessler, J., Dormán, G., Enyedy, É.A., Soós, T., Szatmári, I., Szakács, G., 2022. Structure−activity relationships of 8-hydroxyquinoline-derived Mannich bases with tertiary amines targeting multidrug-resistant cancer. J. Med. Chem. 65, 7729–7745. https://doi.org/10.1021/acs.jmedchem.2c00076.

Patik, I., Székely, V., Német, O., Szepesi, Á., Kucsma, N., Várady, G., Szakács, G., Bakos, É., Özvegy-Laczka, C., 2018. Identification of novel cell-impermeant fluorescent substrates for testing the function and drug interaction of organic anion-transporting polypeptides, OATP1B1/1B3 and 2B1. Sci. Rep. 8, 2630. https://doi.org/10.1038/s41598-018-20815-1.

Pivarcsik, T., Dömötör, O., Mészáros, J.P., May, N.V., Spengler, G., Csuvik, O., Szatmári, I., Enyedy, É.A., 2021. 8-Hydroxyquinoline-amino acid hybrids and their half-sandwich Rh and Ru complexes: synthesis, anticancer activities, solution chemistry and interaction with biomolecules. Int. J. Mol. Sci. 22, 11281. https://doi.org/10.3390/ijms222011281.

Pivarcsik, T., Pósa, V., Kovács, H., May, N.V., Spengler, G., Pósa, S.P., Tóth, S., Yazdi, Z. N., Özvegy-Laczka, C., Ugrai, I., Szatmári, I., Szakács, G., Enyedy, É.A., 2023. Metal complexes of a 5-nitro-8-hydroxyquinoline-proline hybrid with enhanced water solubility targeting multidrug resistant cancer cells. Int. J. Mol. Sci. 24, 593. https://doi.org/10.3390/ijms24010593.

Pivarcsik, T., Tóth, S., Pósa, S.P., May, N.V., Kováts, É., Spengler, G., Kántor, I., Rolya, A., Feczkó, T., Szatmári, I., Szakács, G., Enyedy, É.A., 2024. Organometallic half-sandwich complexes of 8-hydroxyquinoline-derived Mannich bases with enhanced solubility: targeting multidrug resistant cancer. Inorg. Chem. 63, 23983–23998. https://doi.org/10.1021/acs.inorgchem.4c04398, 50.

PropKa server, 2004-2021. A free software developed in 2004-2013 by Jan H. Jensen, Andrew D. Robertson, Hui Li, David M. Rogers. https://www.ddl.unimi.it/vegaol/propka.htm (Accessed 3 March 2025).

Schulte, R.R., Ho, R.H., 2019. Organic anion transporting polypeptides: emerging roles in cancer pharmacology. Mol. Pharmacol. 95, 490–506. https://doi.org/10.1124/mol.118.114314.

Shan, Z., Yang, X., Liu, H., Yuan, Y., Xiao, Y., Nan, J., Zhang, W., Song, W., Wang, J., Wei, F., Zhang, Y., 2023. Cryo-EM structures of human organic anion transporting polypeptide OATP1B1. Cell Res. 33, 940–951. https://doi.org/10.1038/s41422-023-00870-8.

Svoboda, M., Wlcek, K., Taferner, B., Hering, S., Stieger, B., Tong, D., Zeillinger, R., Thalhammer, T., Jäger, W., 2011. Expression of organic anion-transporting polypeptides 1B1 and 1B3 in ovarian cancer cells: relevance for paclitaxel transport. Biomed. PharmacOther 65, 417–426. https://doi.org/10.1016/j.biopha.2011.04.031.

Szakács, G., Paterson, J.K., Ludwig, J.A., Booth-Genthe, C., Gottesman, M.M., 2006. Targeting multidrug resistance in cancer. Nat. Rev. Drug Discovery 5, 219–234. https://doi.org/10.1038/nrd1984.

Tuerkova, A., Ungvári, O., Laczkó-Rigó, R., Mernyák, E., Szakács, G., Özvegy-Laczka, C., Zdrazil, B., 2021. Data-driven ensemble docking to map molecular interactions of steroid analogs with hepatic organic anion transporting polypeptides. J. Chem. Inf. Model. 61, 3109–3127. https://doi.org/10.1021/acs.jcim.1c00362.

Türk, D., Hall, M.D., Chu, B.F., Ludwig, J.A., Fales, H.M., Gottesman, M.M., Szakács, G., 2009. Identification of compounds selectively killing multidrug-resistant cancer cells. Cancer Res. 69, 8293–8301. https://doi.org/10.1158/0008-5472.CAN-09-2422.

Valeur, B., 2001. Molecular Fluorescence Principles and Applications. Wiley-VCH, Weinheim.

Viegas, A., Manso, J., Nobrega, F.L., Cabrita, E.J., 2011. Saturation-transfer difference (STD) NMR: a simple and fast method for ligand screening and characterization of protein binding. J. Chem. Educ. 88, 990–994. https://doi.org/10.1021/ed101169t.

Windt, T., Tóth, S., Patik, I., Sessler, J., Kucsma, N., Szepesi, Á., Zdrazil, B., Özvegy-Laczka, C., Szakács, G., 2019. Identification of anticancer OATP2B1 substrates by an *in vitro* triple-fluorescence-based cytotoxicity screen. Arch. Toxicol. 93, 953–964. https://doi.org/10.1007/s00204-019-02417-6.

Zhang, W., Xiong, X., Wang, F., Li, L., Zhang, Y., Xiao, W., Liu, Y., 2014. Investigation of nitroxoline-human serum albumin interactions by spectroscopic methods. Sci. China Chem. 57, 1690–1695. https://doi.org/10.1007/s11426-014-5230-8.